Steady Flow Through an Abruptly Constricted Channel

by

Roger R. Coroas

B.Sc. University of Havana, Cuba, 1988.

A THESIS SUBMITTED IN PARTIAL FULFILLMENT
OF THE REQUIREMENTS FOR THE DEGREE OF
MASTER OF SCIENCE
in the Department
of
Mathematics & Statistics

SIMON FRASER UNIVERSITY
July 1994

APPROVAL

Name: Roger R. Coroas

Degree: Master of Science

Title of thesis: Steady Flow Through an Abruptly Constricted Channel

Examining Committee: Dr. S. K. Thomason
Chair

Dr. T. Tang
Senior Supervisor

Dr. R. D. Russell

Dr. R. W. Lardner

Dr. A. Karageorghis
External Examiner

Date Approved: July 25, 1994

PARTIAL COPYRIGHT LICENSE

I hereby grant to Simon Fraser University the right to lend my thesis, project or extended essay (the title of which is shown below) to users of the Simon Fraser University Library, and to make partial or single copies only for such users or in response to a request from the library of any other university, or other educational institution, on its own behalf or for one of its users. I further agree that permission for multiple copying of this work for scholarly purposes may be granted by me or the Dean of Graduate Studies. It is understood that copying or publication of this work for financial gain shall not be allowed without my written permission.

Title of Thesis/Project/Extended Essay

Steady flow through an abruptly constricted channel

Author: _____
(signature)

ROGER R. CORDAS
(name)

July 11th, 1994
(date)

Abstract

The steady, two-dimensional, laminar flow of an incompressible fluid through a channel with an abrupt constriction of ratio 2:1 is numerically calculated. The governing equations are solved using a second-order central difference scheme and a fourth-order compact scheme. The Interior Constraint (IC) Method is employed for the numerical treatment of the values at the boundary. The Point Successive Over-Relaxation (SOR) Method is used to solve the discrete equations. Due to the combination of the IC Method at the boundary and the compact scheme at the interior points over-relaxation is now possible. Faster covergence is achieved for higher Reynolds number. An evaluation of different approximations for the boundary vorticity is given. Several flow parameters are calculated and compared to previous works.

Dedication

To my parents, Daisy and Ramón, for their constant support
and
to Jocelyn for her inspiration.

Acknowledgements

I would like to thank all the people who contributed in the completion of this thesis, among whom are:

My senior supervisor Dr. T. Tang, for his guidance and help during this period.

Dr. R. D. Russell and Dr. M. R. Trummer for their friendship and encouragement since the beginning of this program.

Dr. H. Huang for the invaluable discussions and comments.

Dr. G. A. C. Graham and Mr. P. Dobud for making possible my arrival to Simon Fraser University.

My family and friends for their moral support.

Jocelyn Laidlaw for her love and constant understanding.

Stephen and Victoria Trotter for their help.

Antonio and Tatiana for those good meals.

Kostas Korontinis for his unquestionable friendship and for introducing me in the art of ouzo.

Mansilla, Rafa, Leo y Pablo for their support and the good times.

Mrs. S. Holmes for her assistance and the Department of Mathematics and Statistics of Simon Fraser University for financial support.

Contents

Approval ii

Abstract iii

Dedication iv

Acknowledgements v

Contents vii

List of Tables viii

List of Figures ix

1 Introduction 1

2 Governing Equations of Fluid Mechanics 4

2.1 Derivation of Governing Equations 4

2.1.1 Preliminaries 4

2.1.2 Conservation of Mass 6

2.1.3 Conservation of Momentum 7

2.1.4 Conservation of Energy 8

2.1.5 Dimensionless Steady Navier-Stokes Equations . . . 9

2.1.6 Two Dimensional Flows and Vorticity-Stream Function Formulation 10

2.2 Numerical Treatment of the Governing Equations 11
2.2.1 Discretization of Equations 11
2.2.2 The Point Successive Over-Relaxation (SOR) Method 15
3 Flow in a Constricted Channel 17
3.1 Review of Previous Work 17
3.2 The Interior Constraint Method in a Constricted Channel . . 20
3.3 The Vorticity Interior Constraint Method 23
3.4 Numerical Boundary Conditions 25
3.4.1 Boundary Vorticity 25
3.4.2 Boundary Stream Function Extrapolation 27
3.4.3 Outflow Boundary Conditions 28
3.5 Numerical Results 29
3.5.1 Wall Stress and Boundary Vorticity 32
3.5.2 Length of Recirculation Regions 45
4 Conclusions 58
Bibliography 60

List of Tables

3.1 Separation point at upper corner (L_1). 46

3.2 Reattachment point at the upper corner (L_2). 47

3.3 Separation point after the re-entrant corner (L_3). 48

3.4 Reattachment point after the re-entrant corner (L_4). 48

3.5 Stress values on boundary W_1. 51

3.6 Separation values at the upper corner (L_1) for Re=0, 250 and 500. . . 52

3.7 Stress values on boundary W_2. 53

3.8 Reattachment values at the upper corner (L_2) for Re=0, 250 and 500. 54

3.9 Stress values on boundary W_3. 55

3.10 Separation values after the re-entrant corner (L_3) for $Re = 250$ and 500. 56

3.11 Reattachment values after the re-entrant corner (L_4) for $Re = 250$ and 500. 57

List of Figures

2.1 Stencils 12

2.2 Higher order stencils 13

3.1 Domain symmetry. 20

3.2 Grid and computational boundary. 22

3.3 Outlier values for the VIC method. 24

3.4 Characteristic lengths for the flow in a constricted channel. 29

3.5 Iterations number for schemes. 31

3.6 Stress on wall W_1 for different schemes and vorticity boundary approximations. 33

3.7 Stress on wall W_2 for different schemes and vorticity boundary approximations. 35

3.8 Stress on wall W_3 for different schemes and vorticity boundary approximations. 36

3.9 Vorticity distribution on wall W_3 for CB scheme ($Re = 250$ and 500). 37

3.10 Vorticity distribution on wall W_3 for C2 scheme ($Re = 250$ and 500). 38

3.11 Vorticity distribution on wall W_3 for C3 scheme ($Re = 250$ and 500). 39

3.12 Vorticity distribution on wall W_3 for T3 scheme ($Re = 250$ and 500). 40

3.13 Vorticity distribution on wall W_3 for T4 scheme ($Re = 250$ and 500). 41

3.14 Vorticity distribution on wall W_3 for TB scheme ($Re = 250$ and 500). 42

3.15 Oscillations of the vorticity distribution on wall W_1 for scheme T4 . . 43

3.16 Vorticity distribution on walls W_1 and W_3 for schemes C3, T4 and TB. 44

3.17 Streamlines and vorticity contours for scheme T4-(3,2). 45

3.18 Magnification of streamlines and vorticity contours for $Re = 500$ near the re-entrant corner for scheme T4-(3,2). 46

3.19 Characteristic lengths. 49

Chapter 1

Introduction

Fluid dynamics, prior to the computer era, was mainly divided into two branches: theoretical and experimental. The mathematical models resulting from fluid mechanics problems are highly non-linear. Therefore, theoretical solutions are difficult to obtain and mainly found for linear problems. On the other hand to reproduce a physical phenomenon through experiments is a difficult matter. Wind tunnels have been designed to model flows around objects, e.g. cars, airplanes and rockets. Their main disadvantage is cost. Wind tunnels are very expensive to run, and a change in the parameters flow might imply changes in the layout of the experiment. Even for small scale experiments, e.g. flows through channels, the situation is not different. Very sophisticated instruments are needed to measure the velocity of the particles, and the accuracy of this measurements suffer near boundaries.

The introduction of computers resulted in the growth of a completely new field, termed Computational Fluid Dynamics (CFD). This field has led to the development of new mathematical theories for numerical solutions of non-linear differential equations. CFD is close to the experimental branch. Improvements in the computer speed and the search for more efficient numerical solution procedures allow us to model more complex phenomena. But it is still necessary to rely on rigorous mathematical analysis of simpler linearized models, on physical intuition and trial-error procedures.

In Computational Fluid Dynamics the complex non-linear equations are approximated by a system of discrete equations. Many procedures may be used to reduce the continuous equations to a set of discrete ones. Finite differences is one of the most used methods. A *grid* or *mesh* is placed over the domain of interest. At the mesh intersections the finite-difference solutions will be defined. Taylor series are applied at each grid point, and a set of discrete equations are obtained. The order of accuracy of the approximation may vary. Schemes of first and second-order of accuracy are extensively used. A disadvantage is that, for complex flows, very fine meshes are needed and, therefore, the number of discrete equations larger. Usually higher order of accuracy means more grid points for the scheme, except for high order *compact schemes.*

Constricted tubes are found in mechanical devices and in our body (due to atherosclerosis of blood vessel). In this thesis we shall study the flow of a two-dimensional, steady, viscous, incompressible fluid through a constricted channel. Numerical calculations will be made for a channel with constriction ratio 2 : 1. A parabolic velocity profile is imposed upstream, while horizontal flow and constant pressure are assured for the outflow downstream of the channel. Flows in contracting channels have attracted considerable attention. Numerical experiments suggest the presence of a recirculation region downstream. The flow singularity at the re-entrant corner makes the prediction of such a region difficult. The values of the Reynolds number at which the downstream recirculation appears and the wake's dimensions are still open problems. In an effort to solve these problems several flow parameters will be analyzed. We will use a second order scheme and a fourth order compact scheme and compare their performance. A careful examination of the effects of the boundary conditions will be also presented.

In Chapter 2 we will present an overview of the continuous governing equations and their discretization. A derivation of the governing equations of fluid flow, with all the hypotheses involved, will be given in Section 2.1. In Section 2.2 we will give a description of the numerical schemes employed to compute the flow. The solution technique used will also be described.

Chapter 3 begins with a description of the model problem, and a review of the previous work is given in Section 3.1. The Interior Constraint (IC) method is formulated in Section 3.2 for a constricted channel. A variation of the IC method, named the Vorticity Interior Constraint (VIC) method, is proposed in Section 3.3. The boundary conditions employed on this problem are discussed in Section 3.4 and a series of vorticity boundary approximations are also given. Section 3.4 is dedicated to the results. The effects of different vorticity boundary conditions are studied. Characteristic flow parameters are computed, and comparisons with published ones are also given.

Chapter 2

Governing Equations of Fluid Mechanics

2.1 Derivation of Governing Equations

A fluid in motion is characterized by physical magnitudes or quantities such as the velocity, pressure, density, temperature, internal energy, or some other set of variables. Such magnitudes, or dependent variables, are subject to universal physical laws of conservation. A set of mathematical equations governing the dependent variables, based on the physical laws of conservation of mass, momentum and energy, will be derived.

2.1.1 Preliminaries

A fluid consists of many particles in interaction. The behavior of the particles ultimately characterizes the motion of the fluid. One could concentrate on the description of the interaction of such particles and, using the laws of mechanics and probability theory, infer the macroscopic behavior of the fluid. Such an approach is known as the *statistical method*, and is valid for light gases yet incomplete for dense gases and

liquids [5].

Recently a new microscopic approach has been developed. The lattice Boltzmann equation (LBE) method [16, 17], a derivation of the lattice gas automaton method [30], constructs a microworld in which space, time and velocities are all discrete. The particles reside on the lattice's nodes and change their velocities directions according to scattering rules. This method allows the use of fully parallel algorithms and is easily implemented for complex boundary flows.

A different approach is to consider a small volume of continuous fluid, where individual particles are ignored. The microscopic properties of the particles within the volume are averaged to obtain the macroscopic values such as: velocity, pressure, density, or other variables that might describe the fluid. The validity of this *continuous method* is conditional upon the satisfaction of the *continuum hypothesis.* The physical quantities of interest must be spread uniformly over the volume in consideration, and the mean free path of the particles must be small in comparison with the length of the flow field. Only under this continuum hypothesis can the microscopic structure of the fluid be ignored, and the average considered valid.

In this work, the fluid under consideration satisfies the continuum hypothesis. Therefore, the continuous method will be used to state the conservation laws.

The conservation laws could be formulated in either one of the two known coordinate systems: the *Eulerian coordinate system* or the *Lagrangian coordinate system.*

In the Eulerian system a control volume independent of time is fixed in space. The conservation laws are applied to the fluid which passes through the control volume. The dependent variables are functions of the spatial coordinates and time. On the other hand, the Lagrangian system follows a control volume through its motion in the flow. The particles of fluid do not vary, but the shape of the volume might change over time. In this formulation, the spatial variables are not independent of time. The choice of coordinate system varies from author to author, and mainly depends on the problem under consideration. Here the Eulerian coordinate system is used.

Recalling that the independent variables are the spatial coordinates and time,

it is very useful to define the *total derivative*, also known as *convective* or *material derivative*. The total derivative gives the rate of change of any physical magnitude $\mathcal{F}$ when moving with the flow, and it is defined as

$$\frac{D\mathcal{F}}{Dt} \equiv \frac{\partial \mathcal{F}}{\partial t} + (\mathbf{u}\cdot\nabla)\,\mathcal{F} \tag{2.1}$$

where $\mathbf{u}$ is the velocity of the fluid and ∇ the gradient vector.

Here we are only concerned with fluids considered to be Newtonian, incompressible, and for which the changes of temperature in the domain of interest are not significant. The definitions and consequences of these assumptions will be addressed in the following sections.

2.1.2 Conservation of Mass

Consider a fixed control volume V entirely occupied by fluid, and S its surface. The volume V is fixed in space. The particles will enter and leave the volume through the control surface S. These conditions will also apply in the subsequent sections of this work.

The law of conservation of mass states that the mass within any volume varies only as a consequence of the flux across the surface of the volume. The integral form of the conservation of mass applied to the fluid confined in V yields the equation

$$\frac{d}{dt}\int_V \rho\, dV \;=\; -\int_S \rho\, \mathbf{u}\cdot\mathbf{n}\, dS \tag{2.2}$$

where ρ is the fluid density, and $\mathbf{n}$ the outward unit normal of the surface S.

The previous equation holds for any control volume V. A more restrictive form of the conservation of mass can be obtained applying the divergence theorem

$$\frac{\partial \rho}{\partial t} + \nabla\cdot(\rho\mathbf{u}) \;=\; 0 \tag{2.3}$$

which is known as the *continuity equation* in the conservative form. Equation (2.3) is not valid when the quantities involved are not continuous.

A non-conservative form of equation (2.3) can be obtained by expanding the divergence term $\nabla\cdot(\rho\mathbf{u})$ in (2.3) and using the expression for the total derivative

$$\frac{D\rho}{Dt} + \rho\nabla\cdot\mathbf{u} = 0 \tag{2.4}$$

In most liquid flows the total variation of the density ρ may be considered irrelevant and, therefore, assumed to be uniform over the entire fluid. In such cases

$$\frac{D\rho}{Dt} = 0 \tag{2.5}$$

holds and the fluid is said to be *incompressible.* The continuity equation (2.4) then reduces to

$$\nabla\cdot\mathbf{u} = 0. \tag{2.6}$$

2.1.3 Conservation of Momentum

The principle of conservation of momentum states that the rate of change of momentum within a control volume V is equal to the sum of forces acting in such a volume, and it is expressed by

$$\int_V \rho\frac{D\mathbf{u}}{Dt}\,dV = \int_V \rho\mathbf{F}\,dV + \int_V \nabla\cdot\sigma\,dV \tag{2.7}$$

where $\mathbf{u}$ is the velocity, $\mathbf{F}$ the external force acting on the fluid contained in V, and $\sigma = (\sigma_{ij})$ represents the surface stress tensor.

Equation (2.7) holds for any choice of volume V. If the integrands are continuous functions of $\mathbf{x}$ on V the differential equation

$$\rho\frac{D\mathbf{u}}{Dt} = \rho\mathbf{F} + \nabla\cdot\sigma \tag{2.8}$$

holds at every point, and it is known as the *equation of motion.*

As mentioned earlier the fluid is considered to be *Newtonian.* This means that there is a linear relation between the stress acting on the fluid and its rate of deformation. In the case of Newtonian fluids the surface tensor can be written as

$$\sigma_{ij} = -\mathrm{p}\delta_{ij} + 2\mu(e_{ij} - \frac{1}{3}\Delta\,\delta_{ij}) \tag{2.9}$$

where p is the kinematic pressure, δ_{ij} is the Kronecker delta, μ the dynamic coefficient of viscosity, $e_{ij} = \frac{1}{2}(\frac{\partial u_i}{\partial x_j} + \frac{\partial u_j}{\partial x_i})$ the rate of the strain tensor and $\Delta = e_{kk} = \nabla \cdot \mathbf{u}$ the rate of deformation. The dynamic viscosity μ depends mainly on the temperature changes in the flow field. Since we are considering fluids for which the change of temperature is not significant the viscosity μ can be taken to be uniform over the fluid.

The above assumption and the incompressibility of the fluid, expressed through equation (2.6), simplify the expression (2.9). In this way the term $\nabla \cdot \sigma$ in (2.8) can be written as

$$\nabla \cdot \sigma = -\nabla \mathsf{p} + \mu \nabla^2 \mathbf{u}. \tag{2.10}$$

Substitution of (2.10) into (2.8) gives the well known expression of the *Navier-Stokes equations*

$$\rho \frac{D\mathbf{u}}{Dt} = -\nabla \mathsf{p} + \mu \nabla^2 \mathbf{u} + \rho \mathbf{F} \tag{2.11}$$

In the majority of the cases the force $\mathbf{F}$ represents the gravitational force. The term $\rho \mathbf{F}$ in the above equation can be absorbed by the pressure term $\nabla \mathsf{p}$ when the pressure is written as

$$\mathsf{p} = \mathsf{p}_0 + \rho \mathbf{F} \cdot \mathbf{x} + p \tag{2.12}$$

where p_0 is a constant, $\rho \mathbf{F} \cdot \mathbf{x}$ the pressure to balance the force per unit of volume due to $\mathbf{F}$ and p is the pressure arising from the effect of the motion of the fluid- it is known as the *modified pressure* [1].
Substitution of (2.12) into (2.11) gives the formulation of the Navier-Stokes equations in primitive variables

$$\rho \frac{D\mathbf{u}}{Dt} = -\nabla p + \mu \nabla^2 \mathbf{u}. \tag{2.13}$$

Some authors refer to equations (2.13)-(2.6) as the Navier-Stokes equations. The same will be done throughout this work, unless otherwise indicated.

2.1.4 Conservation of Energy

The conservation of energy is an application of the first law of thermodynamics to a control volume V. It states that the change of internal energy is equal to the sum of

the total work done on the system and any heat added. We are interested in fluids in which the temperature is uniform, and therefore the energy equation will not be necessary here.

2.1.5 Dimensionless Steady Navier-Stokes Equations

We are interested in exploring the effects that changing the values of the parameters ρ and μ have on the flow. In this case it is useful to write equations (2.13) and (2.6) in terms of dimensionless variables. Taking L as the reference characteristic length and U as the reference characteristic velocity, the new non-dimensional variables are defined

$$\mathbf{u} = \frac{\mathbf{u}}{U}, \quad \mathbf{x} = \frac{\mathbf{x}}{L}, \quad t = \frac{U}{L}\,t, \quad p = \frac{L}{U^2\rho}\,p. \tag{2.14}$$

Without any loss of generality the same notation for the new variables is kept.
With these new variables the governing equations (2.13)-(2.6) become

$$\frac{D\mathbf{u}}{Dt} = -\nabla p + \frac{1}{Re}\nabla^2\mathbf{u} \tag{2.15}$$

$$\nabla\cdot\mathbf{u} = 0 \tag{2.16}$$

where $Re = \frac{\rho LU}{\mu}$ is the Reynolds number.
The system of equations (2.15)-(2.16) is known as the dimensionless Navier-Stokes equations in primitive form.

In many problems it is important to study the long time behavior of the flow. The steady state equations are obtained by assuming that the physical magnitudes that describe the flow are independent of time. That is, in equations (2.15)-(2.16) the velocity $\mathbf{u}$ and pressure $\mathbf{p}$ are only functions of the position, $\mathbf{u} = \mathbf{u}(\mathbf{x})$, $\mathbf{p} = \mathbf{p}(\mathbf{x})$. In this case the total derivative can be written as

$$\frac{D\mathbf{u}}{Dt} \equiv (\mathbf{u}\cdot\nabla)\,\mathbf{u} \tag{2.17}$$

and equations (2.15) and (2.16) become

$$(\mathbf{u}\cdot\nabla)\,\mathbf{u} = -\nabla p + \frac{1}{Re}\nabla^2\mathbf{u} \tag{2.18}$$

$$\nabla\cdot\mathbf{u} = 0, \tag{2.19}$$

which are the non-dimensional, steady Navier-Stokes equations in primitive variables.

2.1.6 Two Dimensional Flows and Vorticity-Stream Function Formulation

In many cases it is enough to consider planar flows. Due to symmetries in the region of the problem, three-dimensional flows could be studied as two-dimensional flows. This means that the velocity $\mathbf{u}$ is only described by two components $\mathbf{u} = (u, v, 0)$.

It is common practice in fluid dynamics to visualize the flow field by drawing the streamlines. Therefore, it is convenient to introduce the scalar magnitude ψ, named the *stream function*. The stream function is constant along the streamlines and is related to the velocity through the equations

$$u = \frac{\partial \psi}{\partial y} \quad , \quad v = -\frac{\partial \psi}{\partial x} \tag{2.20}$$

which satisfy the continuity equation (2.19). Vortex creation is also a distinctive feature of some flows. It is useful to describe the flow in terms of the distributions of the *vorticity* Ω, defined as

$$\Omega = \frac{\partial v}{\partial x} - \frac{\partial u}{\partial y} \tag{2.21}$$

which is created on the boundary and diffused away by the viscosity. The Navier-Stokes equations in the vorticity-stream function formulation for steady, incompressible, planar flows take the form

$$\nabla^2 \psi = -\Omega \tag{2.22}$$

$$\nabla^2 \Omega = Re \left(\frac{\partial \psi}{\partial y} \frac{\partial \Omega}{\partial x} - \frac{\partial \psi}{\partial x} \frac{\partial \Omega}{\partial y} \right) \tag{2.23}$$

where ∇^2 is the Laplacian operator. Note that the pressure term disappears from the governing equations. The elimination of the vorticity in equations (2.22)-(2.23) leads to the formulation of the Navier-Stokes equations in terms of the stream function

$$\nabla^4 \psi + Re \left(\psi_x \nabla^2 \psi_y - \psi_y \nabla^2 \psi_x \right) = 0 \tag{2.24}$$

where $\nabla^4 = \frac{\partial^4}{\partial x^4} + 2\frac{\partial^4}{\partial x^2 \partial y^2} + \frac{\partial^4}{\partial y^4}$ is the biharmonic operator.

2.2 Numerical Treatment of the Governing Equations

The equations of fluid mechanics are highly nonlinear. Analytical solutions are rarely obtained. The appearance of computers opened a new era in fluid dynamics research. A new field, termed Computational Fluid Dynamics (CFD), has emerged. This field has provided new mathematical methods to solve numerous problems of fluid mechanics. Solutions are obtained by first replacing the derivatives appearing in the governing equations by appropriate discrete approximations and then solving the discrete equations by a suitable numerical method.

2.2.1 Discretization of Equations

Numerous methods have been developed to discretize the governing equations. Among them, the finite difference method is the most commonly used. Finite difference approximations of different orders are found with the use of Taylor expansions of the quantities involved.

Let $f(x)$ be a function defined in $a \leq x \leq b$. A discretization of the interval $[a, b]$ is obtained by considering the set of points $\{x_i = x_0 + ih, i = 0, \ldots, N\}$, with $x_0 = a$, $x_N = b$ and $h = \frac{b-a}{N}$. The discretized values f_i of the function $f(x)$ are obtained by evaluation at the discrete points x_i, i.e. $f_i = f(x_i)$. Different finite difference approximations for the derivatives of $f(x)$ at $x = x_i$ can be obtained from these. For instance the first derivative could be approximated by any of the following expressions

centered second-order

$$\frac{df(x_i)}{dx} = \frac{f_{i+1} - f_{i-1}}{2h} + O(h^2) \tag{2.25}$$

backward first-order

$$\frac{df(x_i)}{dx} = \frac{f_i - f_{i-1}}{h} + O(h) \tag{2.26}$$

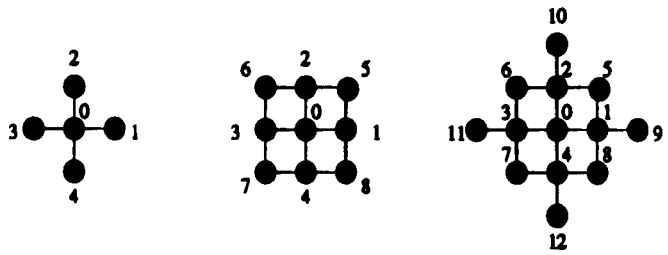

(a) Five Points (b) Compact (c) Nine Points

Figure 2.1: Stencils

forward first-order

$$\frac{df(x_i)}{dx} = \frac{f_{i+1} - f_i}{h} + O(h) \tag{2.27}$$

forward second-order

$$\frac{df(x_i)}{dx} = \frac{-3f_i + 4f_{i+1} - f_{i+2}}{2h} + O(h^2) \tag{2.28}$$

Approximations can also be found for higher order derivatives. The classical difference approximation for the second-order derivative at $x = x_i$ is

$$\frac{d^2f(x_i)}{dx^2} = \frac{f_{i+1} - 2f_i + f_{i-1}}{2h} + O(h^2) \tag{2.29}$$

which has second-order accuracy. Combinations of these finite difference approximations may be put together to obtain the finite difference approximation of the governing equations.

To discretize equations (2.22)-(2.23) consider a uniform mesh in both the x and y directions. Let h be the mesh step size.

The well known central difference or 5-point scheme for the Poisson equation can be obtained using the central difference formula (2.29) in equation (2.22) to obtain

$$\psi_0 = \frac{1}{4}(\psi_1 + \psi_2 + \psi_3 + \psi_4 - h^2\Omega_0) \tag{2.30}$$

where the subscripts $0, 1, 2, 3$ and 4 represent the grid points $(x, y), (x + h, y), (x, y + h), (x - h, y)$ and $(x, y - h)$ respectively (see Figure 2.1a). Similarly the vorticity

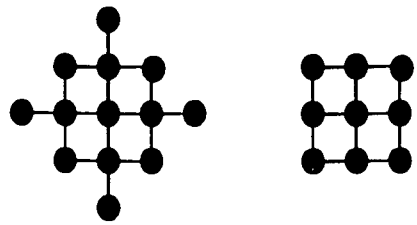

(a) Wide (b) Compact

Figure 2.2: Higher order stencils

equation (2.23) can be approximated by

$$K_1\Omega_1 + K_2\Omega_2 + K_3\Omega_3 + K_4\Omega_4 - K_0\Omega_0 = 0 \tag{2.31}$$

where

$$K_1 = 1 - Re(\psi_2 - \psi_4), \qquad K_2 = 1 + Re(\psi_1 - \psi_3),$$
$$K_3 = 1 + Re(\psi_2 - \psi_4), \qquad K_4 = 1 - Re(\psi_1 - \psi_3),$$
$$K_0 = 4.$$

The discrete equations (2.30)-(2.31) have second-order accuracy.

Higher order schemes for equations (2.22)-(2.23) may be obtained using the same procedure. Generally this procedure will produce wide stencils, and special treatment near the boundaries is needed. For instance, using fourth-order central difference approximations in equation (2.22), a fourth-order scheme for the stencil Figure 2.2a is obtained. A special class of schemes are the compact schemes. A fourth-order compact scheme on the stencil Figure 2.2b is obtained in reference [23], where the grid points $(x+h, y+h), (x-h, y+h), (x-h, y-h)$ and $(x+h, y-h)$, numbered $5, 6, 7$ and 8 respectively, are also considered (see Figure 2.1b). The fourth-order compact scheme for equation (2.22) yields

$$4(\psi_1+\psi_2+\psi_3+\psi_4)+\psi_5+\psi_6+\psi_7+\psi_8+\frac{h^2}{2}(\Omega_1+\Omega_2+\Omega_3+\Omega_4+8\Omega_0)-20\psi_0 = 0 \tag{2.32}$$

which is an example of a Hermitian finite difference method (*Mehrstellenverfahren*) [4].

The approximation for equation (2.23) given in [23] is

$$8(\Omega_1+\Omega_2+\Omega_3+\Omega_4)+2(\Omega_5+\Omega_6+\Omega_7+\Omega_8)-Re\,(S_1+S_2)-\tfrac{Re^2}{4}\,S_3 \\ -[40+2(\psi_1-\psi_3)^2+2(\psi_2-\psi_4)^2]\Omega_0 = 0 \qquad (2.33)$$

where

$$\begin{aligned}
S_1 &= (\psi_2-\psi_4)(\Omega_1-\Omega_3)-(\psi_1-\psi_3)(\Omega_2-\Omega_4),\\
S_2 &= \psi_1(\Omega_8-\Omega_5)+\psi_2(\Omega_5-\Omega_6)+\psi_3(\Omega_6-\Omega_7)+\psi_4(\Omega_7-\Omega_8)\\
&\quad +\psi_5(\Omega_1-\Omega_2)+\psi_6(\Omega_2-\Omega_3)+\psi_7(\Omega_3-\Omega_4)+\psi_8(\Omega_4-\Omega_1),\\
S_3 &= (\psi_1-\psi_3)(\Omega_1-\Omega_3)(\psi_2+\psi_4-2\psi_0)+(\psi_2-\psi_4)(\Omega_2-\Omega_4)(\psi_1+\psi_3-2\psi_0)\\
&\quad +\frac{1}{2}(\psi_1-\psi_3)(\psi_2-\psi_4)(\Omega_5-\Omega_6+\Omega_7-\Omega_8)\\
&\quad -\frac{1}{4}((\psi_1-\psi_3)(\Omega_2-\Omega_4)+(\psi_2-\psi_4)(\Omega_1-\Omega_3))(\psi_5-\psi_6+\psi_7-\psi_8)\\
&\quad -(\psi_1-\psi_3)^2(\Omega_2+\Omega_4)-(\psi_2-\psi_4)^2(\Omega_1+\Omega_3).
\end{aligned}$$

Finite difference approximations of equation (2.24) are obtained on a wider stencil (see Figure 2.1c). The grid points $(x+2h,y),(x,y+2h),(x-2h,y)$ and $(x,y-2h)$ are now needed, and they are numbered $9,10,11$ and 12, respectively (see, e.g., [21]). On this stencil the scheme for equation (2.24) is

$$\nabla_h^4\psi_{ij} = Re\; JB_h(\psi_{ij}) \qquad (2.34)$$

where

$$\begin{aligned}
\nabla_h^4\psi_{ij} &= 8(\psi_1+\psi_2+\psi_3+\psi_4)-2(\psi_5+\psi_6+\psi_7+\psi_8)\\
&\quad -(\psi_9+\psi_{10}+\psi_{11}+\psi_{12})-20\psi_0,\\
JB_h(\psi_{ij}) &= \frac{1}{4}(S_1-S_2)
\end{aligned}$$

and

$$\begin{aligned}
S_1 &= (\psi_1-\psi_3)[\psi_5+\psi_6-\psi_7-\psi_8+\psi_{10}-\psi_{12}-4(\psi_2-\psi_4)],\\
S_2 &= (\psi_2-\psi_4)[\psi_5-\psi_6-\psi_7+\psi_8+\psi_9-\psi_{11}-4(\psi_1-\psi_3)].
\end{aligned}$$

The term $\nabla_h^4\psi_{ij}$ is a discretization of $\nabla^4\psi$ and the term $JB_h(\psi_{ij})$ is a discretization of $JB(\psi)=\psi_x\nabla^2\psi_y-\psi_y\nabla^2\psi_x$. This scheme provides an approximation of second-order for equation (2.24).

2.2.2 The Point Successive Over-Relaxation (SOR) Method

Once the governing equations are discretized, it is necessary to employ a suitable numerical method to solve the system of discrete equations. Several methods are available. Direct methods are, generally, memory consuming and difficult to implement for complex geometries. Iterative methods are more frequently used in computational fluid dynamics.

The Point SOR method is an iterative method that can be used to solve discretized elliptic problems. This method is very easy to implement, requires very little memory and is one of the most efficient point-iterative procedures for large systems of equations. A sufficient condition for the convergence of this method is ***diagonal dominance.***

Let $A\psi = \mathbf{b}$ be a system of equations obtained after the discretization of a elliptic equation, e.g., equation (2.22). The condition of diagonal dominance is that

$$|a_{ii}| \geq \sum_{i \neq j}^{n} |a_{ij}| \tag{2.35}$$

for all $i = 1, \ldots, n$.

The SOR method, given the most recent calculated value ψ_0^*, makes a correction using the the value calculated in the previous iteration

$$\psi_0^{n+1} = \omega \psi_0^* + (1 - \omega)\psi_0^n \tag{2.36}$$

where ω is the relaxation parameter. We refer to this as over-relaxation when $1 < \omega < 2$. In some problems under-relaxation, $0 < \omega < 1$, is employed. In the literature both cases are often refer to as the SOR method. The choice of an optimal value for ω (denoted by ω_{opt}) could reduce considerably the number of iterations. For Laplace's equation on a rectangular domain with Dirichlet boundary conditions, an expression for ω_{opt} has been obtained (see, e.g., [27]). For complex elliptic problems it is not possible to obtain ω_{opt} in advance. In those cases, some numerical experimentation should be helpful in identifying the best values of ω. Numerical experiments generally indicate that it is better to over-estimate the value of ω_{opt} rather than under-estimate

it. Similar remarks apply for the vorticity

$$\Omega_0^{n+1} = \lambda\Omega_0^* + (1-\lambda)\Omega_0^n \tag{2.37}$$

where λ is the relaxation parameter and Ω_0^* is calculated from any of the given approximations.

The iterative process (2.36)-(2.37) is stopped when, for a given value ϵ, the conditions

$$\|\psi^{n+1} - \psi^n\| < \epsilon, \tag{2.38}$$

$$\|\Omega^{n+1} - \Omega^n\| < \epsilon \tag{2.39}$$

are satisfied at every interior mesh point.

As mentioned earlier, explicit boundary conditions for the vorticity are not usually provided. Some kind of approximation formula may be used to determine the boundary vorticity values at each iteration, as it will be discussed later. It is a usual procedure to use a boundary damping parameter δ to achieve or accelerate convergence of the iterative process. In this case the values of the boundary vorticity are given by

$$\Omega_B^{n+1} = \delta\Omega_B^n + (1-\delta)\Omega_B^* \tag{2.40}$$

where $0 < \delta < 1$ is the damping parameter and Ω_B^* is the boundary vorticity computed.

Chapter 3

Flow in a Constricted Channel

3.1 Review of Previous Work

Flows in constricted tubes are frequently found in many technological devices and even inside the human body, as in the case of blood vessels with stenoses. Such flows exhibit complex patterns. Recirculating flow is usually found before and after the constriction. This behavior is, in most cases, not desirable. A good understanding of the flow structure is vital to prevent unwanted behavior and properly control the process.

Flows in channels with a sudden contraction have been studied by several authors [11, 10, 8, 20, 22, 15, 18] and present numerous interesting problems. A downstream wake is observed for a certain value of the Reynolds number Re and higher values. The fine structure of the flow is not well known yet. The singularity of the flow at the re-entrant corner makes it difficult to predict the length of the downstream recirculation region and the value of Re at which first separation appears.

The first effort to numerically study separating flows in channels was produced by Greenspan [11] and Friedman [10]. They investigated the flow in a channel with a square constriction on one wall. Using a finite difference discretization for the governing equations in the stream function-vorticity formulation, Friedman [10] obtained

the solution for $0 \leq Re \leq 1000$. The mesh sizes $h = \frac{1}{10}, \frac{1}{20}$ and $\frac{1}{40}$ were not fine enough to capture the recirculation area after the re-entrant corner. However, a separation vortex upstream of the step, not previously described by Greenspan [11], was discovered.

Later, Dennis and Smith [8] focused their attention on the upstream step. Numerical solutions for the flow of an incompressible fluid, through a channel with a constriction in form of an infinite step, were obtained. A second-order scheme developed by Dennis and Hudson [7] was employed to solve the governing equations. This scheme introduces artificial viscosity at each mesh point. The local truncation error is $O(h^2Re^2)$, and second-order accuracy is guaranteed only if $hRe << 1$. It is therefore necessary to use a small grid size to obtain dependable results for large values of Re. Uniform meshes with sizes $h = \frac{1}{10}, \frac{1}{20}, \frac{1}{40}, \frac{1}{60}$ and $\frac{1}{80}$ were employed to find solutions for Reynolds numbers up to 2000. Dennis and Smith inferred that the recirculation appears primarily at a value of Re between 100 and 500, but they failed to produce it in their calculations.

The effects of Dennis-Hudson's artificial viscosity scheme in the accuracy of the solution was explored by Hunt [20]. After discretization of the governing equations, Hunt eliminated the vorticity by substitution and obtained a system of equations in terms of the stream function. A non-uniform grid with a high concentration of mesh points near the corner was used. Reynolds numbers up to 2000 were considered. His results predicted a downstream recirculation region starting at $Re = 250$ not found in previous calculations. Hunt, as previously reported by Bramley and Sloan [3], stated that Dennis-Hudson's scheme is less accurate if the artificial viscosity is added.

Karageorghis and Phillips [22] solved the Navier-Stokes equations in the stream function formulation by using spectral approximations for $0 \leq Re \leq 500$. Collocation points are densely distributed in a vicinity of the corner and near the walls. They reported that the downstream wake first appears at around $Re \approx 175$ and that the separation occurs at the corner and not to the right as predicted by Hunt [20]. They found a second vortex at the upper corner upstream of the step, which is in agreement with Moffatt's theory [25].

Hawken *et al.* [15] studied this contraction flow using a finite element discretization for the governing equations in primitive variables. A high concentration of elements is placed close to the re-entrant corner. Even though they failed to visualize the downstream vortex, the velocity gradient revealed a very thin recirculation region at $Re = 250$ near the corner. They suggested that separation occurs to the right of the corner. Their downstream wake reattachment values are slightly higher than Hunt's values, but smaller than Karageorghis and Phillips'.

In a more recent paper Huang and Seymour [19] employed the Interior Constraint (IC) method, proposed by Huang [18], to solve this problem. A computational boundary is set up near the physical boundary and the use of vorticity values at the physical boundary is avoided. Both uniform and non-uniform grids were employed in calculations with a fine mesh size $h = \frac{1}{200}$. The non-uniform grid is generated by local coordinate transformation, mapping the channel into a unit square before discretization. Huang and Seymour found that the uniform grid works better than the non-uniform grid when the central difference scheme is used. They predicted a downstream recirculation region starting at $Re = 250$. The separation occurs after the corner, as predicted by Hunt [20] and Hawken *et al.* [15], and moves towards the corner when Re increases.

The treatment of the singularity of the vorticity function at the sharp corner has also been a concern. Roache [27] reviews different methods of handling the corner vorticity. A local coordinate transformation near the re-entrant corner was proposed by Dennis and Smith [8]. The finite difference approximation was applied along lines with 45° of inclination with respect to the main grid lines, to avoid the use of the vorticity at the corner. The use of the vorticity at the boundary was avoided by Hunt [20], who used the equations in terms of the stream function only. But as noted by him the singularity of the vorticity leads to a singularity of the second derivative of the stream function, that might affect the accuracy of the results. Hunt also proposed the use of Moffatt's expansion [25], successfully employed by Bramley and Dennis [2] in a branching channel.

The vorticity does not appear in Hawken *et al.* [15] equations, since the primitive

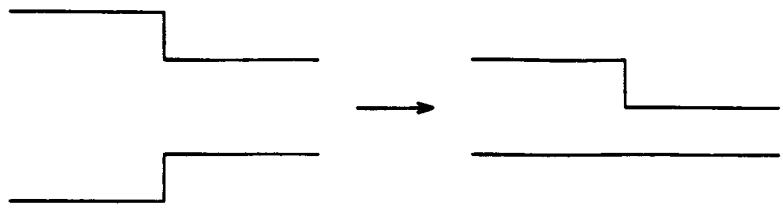

Figure 3.1: Domain symmetry.

variable formulation is employed. But the calculations are affected by singularities in the derivatives of the velocity components. The vorticity values at the boundary are not employed by Karageorghis and Phillips [22] and Huang and Seymour [19] in their calculations, but they are used to predict separation and reattachment lengths. In reference [14] Gupta *et al.* obtained a power series solution for the cavity problem near the corner, valid for small Reynolds numbers. In a recent paper Ma and Ruth [24] developed a vorticity-circulation method to treat the singularity of the vorticity at the corner. A review of some other methods is also given in their paper.

In the present work the Interior Constraint (IC) Method, proposed by Huang [18], and a variant of it are considered. Finite difference discretizations of the stream function-vorticity formulation of the governing equations on uniform grids are chosen. The system of discretized equations is solved by means of an iterative method. Once convergence is reached, various wall vorticity formulae are considered to calculate parameters that characterize this flow.

3.2 The Interior Constraint Method in a Constricted Channel

We are interested in the simulation of the flow of an incompressible fluid in a constricted channel, with constriction ratio 2 : 1. Considering that the flow is symmetric with respect to the mid line of the channel, we can restrict our calculations to the upper half of the channel (see Figure 3.1). The constricted wall of the channel is W_1= $\{y = 1, \text{ for } x \leq 0\}$, W_2= $\{x = 0, \text{ for } \frac{1}{2} \leq y \leq 1\}$ and W_3= $\{y = \frac{1}{2}, \text{ for } x \geq 0\}$,

and $y = 0$ is a symmetry wall. The upstream and downstream boundaries are set at $x = x_{in}$ and $x = x_{out}$ respectively. A parabolic Poiseuille flow is imposed on the upstream boundary.

The Navier-Stokes equations formulated in terms of the stream function and vorticity are the governing equations

$$\nabla^2\Omega = Re\, J(\psi,\Omega) \tag{3.1}$$

$$\nabla^2\psi = -\Omega \tag{3.2}$$

where $J(\psi,\Omega) = \psi_y\Omega_x - \psi_x\Omega_y$ and the wall boundary conditions

$$\psi = 0,\ \Omega = 0, \quad \text{on } y = 0, \tag{3.3}$$

$$\psi = 1, \frac{\partial\psi}{\partial y} = 0, \quad \text{on } y = 1 \text{ for } x \le 0 \text{ and } y = \frac{1}{2} \text{ for } x \ge 0, \tag{3.4}$$

$$\psi = 1, \frac{\partial\psi}{\partial x} = 0, \quad \text{on } x = 0 \text{ for } \frac{1}{2} \le y \le 1, \tag{3.5}$$

the inflow boundary conditions

$$\psi = \frac{1}{2}\, y(3 - y^2), \tag{3.6}$$

$$\Omega = 3y, \tag{3.7}$$

$$\text{on } x = x_{in} \text{ and } 0 \le y \le 1,$$

and the outflow boundary conditions

$$\frac{\partial\psi}{\partial x} = 0, \tag{3.8}$$

$$\frac{\partial\Omega}{\partial x} - Re\, \frac{\partial\psi}{\partial y}(\Omega + \frac{\partial^2\psi}{\partial y^2}) = 0, \tag{3.9}$$

$$\text{on } x = x_{out} \text{ and } 0 \le y \le \frac{1}{2}.$$

The condition (3.9) is obtained from the governing equations imposing $v = 0$, $\frac{\partial v}{\partial y} = 0$ and $\frac{\partial p}{\partial y} = 0$, which give horizontal flow and constant pressure along the outflow boundary.

A uniform mesh is set up with N and M grid points in the x and y directions, respectively. The mesh size is taken to be $\frac{1}{M}$. The vertical wall W_2 is located at the

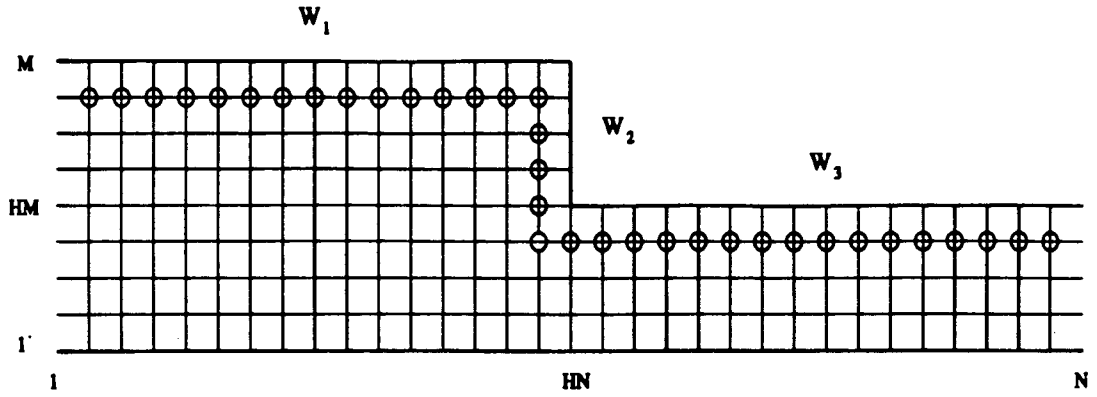

Figure 3.2: Grid and computational boundary.

grid line HN, while the horizontal wall after the contraction W_3 is located at the HM grid line. The interior constraint method introduces a computational boundary parallel to the contracting wall. The marked grid points with $\oplus$ in Figure 3.2 represent the computational boundary for this method.

Two different finite difference schemes, second-order central differences [27] and a fourth-order compact scheme [23], will be employed to discretize the governing equations at the interior points.

Let us consider (x_i, y_j) as an interior grid point, then $\psi_{ij} = \psi(x_i, y_j)$ and $\Omega_{ij} = \Omega(x_i, y_j)$ are the discretized values of the stream function and the vorticity at the grid point, respectively. The discretized equations are as follow

$$\nabla_h^2 \Omega_{ij} = Re J_h(\psi_{ij}, \Omega_{ij}), \tag{3.10}$$

$$\nabla_h^2 \psi_{ij} = -\Omega_{ij}, \tag{3.11}$$

$$\text{for } i = 2, \ldots, HN-1, \quad j = 2, \ldots, HM-1,$$

$$\text{and } i = HN, \ldots, N-1, \quad j = 2, \ldots, HM-2,$$

$$\text{and } i = 2, \ldots, HN-2, \quad j = HM, \ldots, MM-2,$$

where ∇_h^2 and J_h are discretizations of ∇^2 and J respectively.

The vorticity values on the computational boundary are given by discretization of

the stream function equation

$$\begin{aligned} &\Omega_{ij} = -\nabla_h^2 \psi_{ij}, \\ &\text{for } i = 2, \ldots, HN-1,\ j = M-1, \\ &\text{and } i = HN1,\ j = HM, \ldots, M-2, \\ &\text{and } i = HN, \ldots, HN-1,\ j = HM-1. \end{aligned} \tag{3.12}$$

The one sided discretizations of the ***non-slip*** conditions on the physical boundary are used to interpolate the values of the stream function at the computational boundary

$$\begin{aligned} &D_h^x \psi_{ij} = 0 \\ &\text{for } i = HN,\ j = HM, \ldots, M-1 \end{aligned} \tag{3.13}$$

and

$$\begin{aligned} &D_h^y \psi_{ij} = 0 \\ &\text{for } i = 2, \ldots, HN-1,\ j = M \\ &\text{and } i = HN, \ldots, HN-1,\ j = HM \end{aligned} \tag{3.14}$$

where $D_h^x \psi_{ij}$ and $D_h^y \psi_{ij}$ are the discretization at the grid point (x_i, y_j) of ψ_x and ψ_y, respectively. If, for instance, a second-order approximation for $\psi_x = 0$ is employed at the physical boundary, the value of the stream function at the computational boundary ψ_{i-1j} can be isolated from the expression $D_h^x \psi_{ij} = 3\psi_{ij} - 4\psi_{i-1j} + \psi_{i-2j} = 0$.

3.3 The Vorticity Interior Constraint Method

The purpose of the IC method is to avoid using the boundary vorticity values in the calculations. The values of the stream function at the computational boundary are obtained by interpolation using the non-slip conditions at the wall. Here we will propose a variation of the IC method, which will be named the Vorticity Interior Constraint (VIC) method. The computational boundary is kept when vorticity values are calculated. For the stream function, the grid points adjacent to the contracting wall are

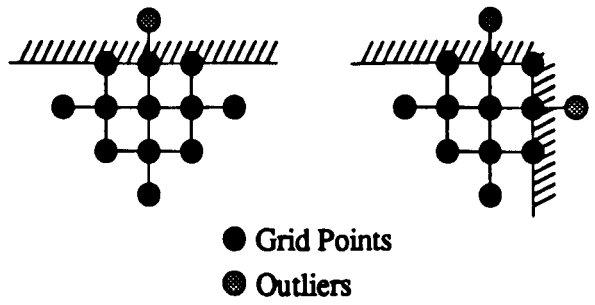

Figure 3.3: Outlier values for the VIC method.

now treated as interior points. The grid point $\ominus$ is now added to the computational boundary.

The biharmonic formulation [27] of the Navier-Stokes equations (2.24) is now imposed at these grid points and interpolation from the non-slip condition is no longer necessary. The non-slip conditions at the wall are now used to eliminate the outlier values (see Figure 3.3).

For the VIC method the discretized vorticity values at the computational boundary are calculated as in (3.12), and the stream function values are calculated as follows:

$$\nabla_h^4 \psi_{ij} = Re\ JB_h(\psi_{ij}), \tag{3.15}$$

$$D_h^x \psi_{ij} = 0, \tag{3.16}$$

$$\text{for } i = HN,\ j = HM, \ldots, M-1$$

and (3.17)

$$\nabla_h^4 \psi_{ij} = Re\ JB_h(\psi_{ij}), \tag{3.18}$$

$$D_h^y \psi_{ij} = 0, \tag{3.19}$$

$$\text{for } i = 2, \ldots, HN-1,\ j = M$$

$$\text{and } i = HN, \ldots, HN-1,\ j = HM$$

where ∇_h^4 and JB_h are defined as before. Note that this will give second-order accuracy for the stream function for points adjacent to the contracting wall.

3.4 Numerical Boundary Conditions

3.4.1 Boundary Vorticity

As mentioned earlier, if the IC or the VIC methods are used, the vorticity values on the wall are not needed to calculate the flow inside the domain. Nevertheless, some characteristic parameters, such as reattachment points, are usually provided to establish the validity of the solution. These parameters can be obtained from the values of the vorticity at the boundary. Roache [27] mentioned the importance of choosing adequate formulae for the vorticity boundary. A wide variety of boundary approximation formulae were tested by Gupta and Manohar [12] for the square cavity problem.

It is our concern that the comparison parameters provided might depend on the boundary vorticity formula used, even though such formulae are not used throughout the calculations. A survey of different formulae for the vorticity at the wall is produced. Careful comparisons are made to determine the nonreliable approximations.

Let us assume that the grid point (x_i, y_j) lies on the boundary $W_1 = \{y = 1 \text{ and } x_{in} \leq x \leq 0\}$, that is $j = M$ and $1 \leq i \leq HN$.

One of the first boundary vorticity formulae was produced by Thom [28]

$$\Omega_{iM} = -\frac{2}{h^2}\left[\psi_{iM-1} - \psi_{iM}\right] + O(h). \tag{3.20}$$

This first-order formula has been used extensively in flow calculations and often gives results as accurate as higher order formulae [27].

The second-order formula, developed by Woods [31], has been widely used

$$\Omega_{iM} = -\frac{3}{h^2}\left[\psi_{iM-1} - \psi_{iM}\right] - \frac{1}{2}\Omega_{iM-1} + O(h^2). \tag{3.21}$$

It also involves a vorticity value adjacent to the boundary. Some unstabilities and low convergence rate have been reported for this formula.

Here we will also consider a whole class of first-order and second-order formulae, called the $(p, 0)$ and (p, q) formulae, respectively, proposed in reference [12].

The first-order $(p,0)$ formulae are defined by

$$\Omega_{iM} = -\frac{2}{h^2} p^{-2} \left[\psi_{iM-p} - \psi_{iM}\right] + O(h) \tag{3.22}$$

Note that $p = 1$ gives us the well known Thom's formula.
The second-order (p,q) formulae are given by

$$\Omega_{iM} = -\frac{2}{h^2} \alpha \left[q^3\psi_{iM-p} + p^3\psi_{iM-q} - (p^3 - q^3]\psi_{iM}\right) + O(h^2) \tag{3.23}$$

where p and q are integers, $p > 0$, $q > 0$, $p \neq q$ and $\alpha = p^{-2}q^{-2}(p-q)^{-1}$.

In this work we will consider from the class (3.22) the first-order formulae

$(2,0)$

$$\Omega_{iM} = -\frac{1}{2h^2} \left[\psi_{iM-2} - \psi_{iM}\right] + O(h), \tag{3.24}$$

$(3,0)$

$$\Omega_{iM} = -\frac{2}{9h^2} \left[\psi_{iM-3} - \psi_{iM}\right] + O(h), \tag{3.25}$$

and from the second-order class (3.23) the formulae

$(2,1)$

$$\Omega_{iM} = -\frac{1}{2h^2} \left[-\psi_{iM-2} + 8\psi_{iM-1} - 7\psi_{iM}\right] + O(h^2), \tag{3.26}$$

$(3,1)$

$$\Omega_{iM} = -\frac{1}{9h^2} \left[-\psi_{iM-3} + 27\psi_{iM-1} - 13\psi_{iM}\right] + O(h^2), \tag{3.27}$$

$(3,2)$

$$\Omega_{iM} = -\frac{1}{18h^2} \left[-8\psi_{iM-3} + 27\psi_{iM-2} - 19\psi_{iM}\right] + O(h^2), \tag{3.28}$$

$(4,3)$

$$\Omega_{iM} = -\frac{1}{72h^2} \left[-27\psi_{iM-4} + 64\psi_{iM-3} - 37\psi_{iM}\right] + O(h^2). \tag{3.29}$$

Gupta and Manohar [12] pointed out that for larger values of p and q convergence is achieved faster but the solution becomes less accurate. In our work the boundary approximations of the vorticity will not affect the convergence process, since they are not used throughout the calculations. However they are expected to affect the accuracy of the flow parameters calculated afterward.

In previous works the sizes of the recirculation regions are taking as comparison parameters. These values depend strongly on the boundary vorticity approximation used, since they are usually calculated using the boundary coordinate where the vorticity is equal to zero. Isolated values of the vorticity are not reliable parameters to measure accuracy [12]; therefore, one should provide some other parameters for comparison purposes.

As an alternative parameter the total shear stress on the contracting wall is calculated. Here a non-dimensional value of the shear stress, introduced in [12], will be used. On the contracting walls W_1, W_2 and W_3 the shear force is defined by

$$F_1 = \int_{x_{in}}^{0} \Omega|_{y=1} \; dx, \tag{3.30}$$

$$F_2 = \int_{\frac{1}{2}}^{1} \Omega|_{x=0} \; dy, \tag{3.31}$$

$$F_3 = \int_{0}^{x_{out}} \Omega|_{y=\frac{1}{2}} \; dx. \tag{3.32}$$

As shown in [12], the shear stress at the wall reflects the accuracy of the vorticity boundary approximations employed.

3.4.2 Boundary Stream Function Extrapolation

As mentioned earlier when the IC method is used the value of the stream function at the computational boundary are extrapolated from the non-slip boundary conditions.

The most interesting features of the flow in a channel with a contraction appear at the contracting wall. In reference [19], one sided second-order approximation formulae are used to approximate the non-slip conditions and second-order central differences are used at the interior points. Higher order approximations for the non-slip conditions are proposed and used here.

Assuming that our boundary point lies on the upstream contracting wall W_1, second, third and fourth-order one sided formulae [6] are defined by

$$D_h^y \psi_{iM} = \frac{1}{2h}\left[-3\psi_{iM} + 4\psi_{iM-1} - \psi_{iM-2}\right] + O(h^2), \tag{3.33}$$

$$D_h^y \psi_{iM} = \frac{1}{6h}[-11\psi_{iM} + 18\psi_{iM-1} - 9\psi_{iM-2} + 2\psi_{iM-3}] + O(h^3), \quad (3.34)$$

and (3.35)

$$D_h^y \psi_{iM} = \frac{1}{12h}[-25\psi_{iM} + 48\psi_{iM-1} - 36\psi_{iM-2} + 16\psi_{iM-3} - \quad (3.36)$$
$$-3\psi_{iM-4}] + O(h^4).$$

For the second-order central differences method, approximations (3.33)-(3.34) are employed in the calculations. For the fourth-order compact method formulae (3.34)-(3.35) are used.

In the case of the VIC method the second-order approximation for the biharmonic operator [21] is used for both interior methods. Higher order approximations, e.g. the compact schemes proposed by Wittkopf [29], could also be used.

3.4.3 Outflow Boundary Conditions

One might think that the outflow boundary condition will be the easiest to impose, setting the end of the channel far away from the constriction. It has been found numerically that instabilities might propagate upstream and invalidate the solution if the outflow conditions are too restrictive [27]. On the other hand, the use of large values for x_{out} increases the cost of the calculations and, to reduce the cost, some kind of domain transformation will be needed. Therefore, it is very important to use economical outflow boundary conditions.

A reasonable attempt would be to impose Poiseuille flow far downstream. Our numerical experiments show that independently of the value of x_{out} an abrupt transition in the flow is observed at the end of the channel. The horizontal flow condition is not satisfied, since Poiseuille flow downstream is far too restrictive. A less restrictive downstream condition, $\psi_x = 0$ and $\Omega_x = 0$, was proposed by Paris and Whitaker [26]. The first equation gives horizontal flow downstream but Roache [27], in numerical experiments, found the second equation might destabilize the solution.

In the present work conditions (3.8)-(3.9), formulated by R. E. Meyer and used

by Greenspan [11] and Friedman [10], are employed. Horizontal flow is guaranteed downstream by equation (3.8) and equation (3.9) gives constant pressure along the outflow boundary at steady state.

3.5 Numerical Results

The calculations were carried out for Reynolds number up to 500 on a uniform mesh with size $h = \frac{1}{200}$. The upstream and downstream boundaries were set at $x_{in} = -2$ and $x_{out} = 2$, respectively.

Several characteristic parameters are produced for this flow. The length, L_1, of the upper corner vortex and its width L_2 , the separation and reattachement values of the downstream wake, L_3 and L_4, are all measured from the corners (see Figure 3.4). The stress on each wall section of the contracting boundary is also monitored. Numerical experiments show that the parameters L_3 and L_4 are sensitive to the grid size, and L_1 and L_2 behave in a more stable way.

For comparison purposes the outflow boundary condition was also set at $x_{out} = 3$. Calculations were made using the fourth-order compact method with extrapolation of fourth-order. For the Reynolds number employed significative differences in the flow parameters were not found, as suggested in [8] and [19].

The solution is calculated for Re with increments of 50. For $Re = 0$ the initial approximation is taken to be zero at every interior point. For $Re > 0$ the solution

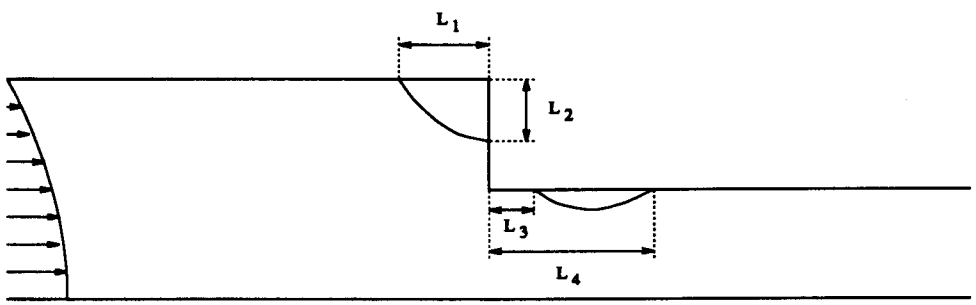

Figure 3.4: Characteristic lengths for the flow in a constricted channel.

calculated for previous Reynolds number is used as initial approximation. This means, for example, that the converged numerical solution for $Re = 400$ is used as the initial approximation to calculate the solution for $Re = 450$. Continuation on Re is necessary because for large values of Re the iterative process is not robust enough to converge from an initial approximation of zero everywhere.

The iterative process considered requires the use of relaxation parameters. For both schemes, central differences and compact, the boundary vorticity damping parameter δ was set at 0.6.

At the interior points, when using the central differences scheme, overrelaxation is possible for the stream function equation and ω was set to be 1.4 throughout the calculations. Under-relaxation is necessary for the vorticity equation. Initially the value of λ is set at 0.8, but the iteration process becomes divergent for $Re = 450$. For $450 \leq Re \leq 500$ the value of λ is set at 0.7 to ensure convergence.

The compact scheme allows the use of over-relaxation for both equations, and parameters were set at $\omega = 1.5$ and $\lambda = 1.3$ throughout the calculations.

Another relaxation parameter is needed for the VIC method. The values of the stream function at the grid points adjacent to the contracting wall are relaxed using $\beta = 0.6$.

The iterative process is stopped when conditions (2.38)-(2.39) are satisfied at the interior points. The value of ϵ is set as 0.0005 and

$$\|\psi^{n+1} - \psi^n\| = \sum_{ij} |\psi_{ij}^{n+1} - \psi_{ij}^n|. \tag{3.37}$$

Figure 3.5 shows the number of iterations required for the iterative process to converge for the schemes at different Reynolds numbers. Recall that continuation on the Reynolds number is used to calculate the solution. The solution for $Re = 0$ is calculated from an initial interior approximation of zero everywhere. This is the reason why the iteration number for $Re = 0$ is considerably higher than for the rest. Note that the compact scheme requires less iterations overall, but the cost per iteration is higher than for the central difference scheme. A good feature of the compact scheme

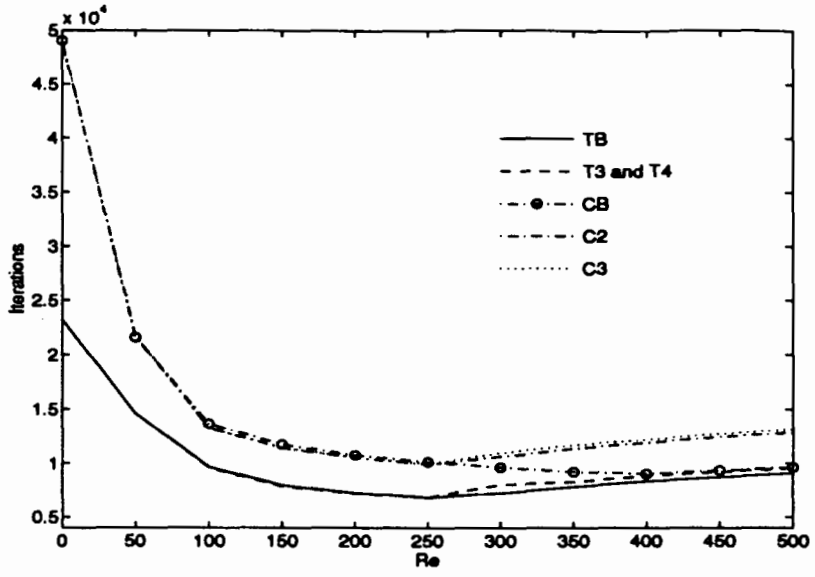

Figure 3.5: Iterations number for schemes.

is that solutions can be found for larger values of the Reynolds number. The central difference scheme is limited in that respect [13].

The following abbreviations are considered in this and the following sections:

C2: Central differences scheme, with second-order approximation for the stream function on the boundary.

C3: Central differences scheme, with third-order approximation for the stream function on the boundary.

T3: Fourth order compact scheme, with third-order approximation for the stream function on the boundary.

T4: Fourth order compact scheme, with fourth-order approximation for the stream function on the boundary.

CB: The VIC method for central differences scheme.

TB: The VIC method for fourth-order compact scheme.

BC1: Thom's formula for the boundary vorticity.

BC2: Woods' formula for the boundary vorticity.

BC3: (2,0) formula for the boundary vorticity.

BC4: (3,0) formula for the boundary vorticity.

BC5: (2,1) formula for the boundary vorticity.

BC6: (3,1) formula for the boundary vorticity.

BC7: (3,2) formula for the boundary vorticity.

BC8: (4,3) formula for the boundary vorticity.

3.5.1 Wall Stress and Boundary Vorticity

Gupta and Manohar [12] found that the numerical boundary vorticity might affect the flow structure. It is our interest to find the most appropriate vorticity formula for every interior scheme used in the calculations. A theoretical solution is not known for the flow in a constricted channel. Reference papers provide, as comparison parameters, the lengths of the upstream and downstream wakes. These parameters are calculated from isolated values of the vorticity or the velocity. As mentioned before, isolated values should not be used to test accuracy. They should be used in combination with more reliable parameters. Gupta and Manohar [12] mentioned that, even though isolated values of the vorticity on the boundary are not reliable, the integral over the boundary is a reliable parameter. This integral gives a non-dimensional stress on the wall. The stress on each of the three sections of the contracting wall is calculated. The vorticity at the re-entrant corner is considered bivalued and therefore discontinuous.

Most figures and tables shown in this chapter make use of abbreviations for schemes and boundary vorticity formulae. Refer to pages 32-33 for full description of abbreviations.

Figure 3.6 shows the wall stress values F_1 on W_1 for $Re \leq 500$. Each plot corresponds to a different numerical scheme. The stress calculated with different boundary vorticity approximations is plotted.

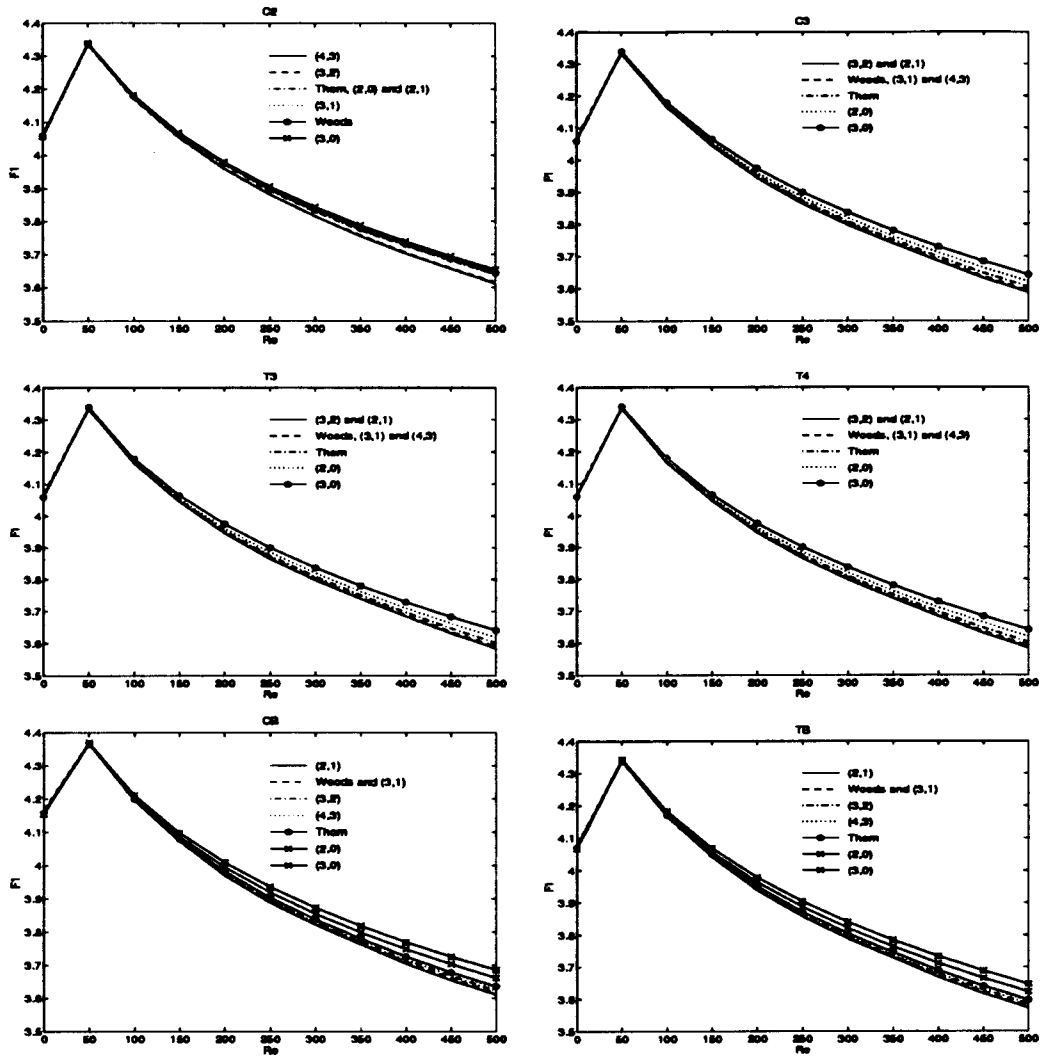

Figure 3.6: Stress on wall W_1 for different schemes and vorticity boundary approximations.

It is obvious that there are no significant differences for $Re \leq 100$. This means that all the boundary vorticity approximations should produce similar results for Reynolds numbers up to 100.

Significant differences are not found for L_1 and L_2 among the different boundary formulae when $Re \leq 100$. On this wall the stress decreases as the order of the boundary vorticity formulae increase. There is a clear separation between first and second-order conditions. In the first-order class, Thom's condition gives the smallest stress values overall, and they are close to the values given by the second-order formulae for $Re \leq 250$.

The (3,2) formula gives the lowest values of the wall stress for the schemes C3, T3 and T4. For schemes CB and TB the lowest stress values is given by the (2,1) formula, and scheme C2 is given by the (3,2) formula.

The stress F_1 and vortex length values L_1 for $Re = 0, 250$ and 500 are given in Table 3.5 and Table 3.6, respectively.

Plots of the stress F_2 on wall W_2 are given in Figure 3.7. It is observed that the stress values on W_2 increase as the accuracy of the boundary formula increases. For F_2 the boundary conditions keep the same relation of order as for F_1, except for scheme C2 where formula (3,2) gives now the maximum stress. In this figure there is a bigger difference among the values given by the different formulae.

The first-order formulae give smaller values for F_2 than the second-order formulae. Once again Thom's condition gives the best values among the first-order class formulae. The values for F_2 for the VIC method are larger than the values obtained for the other schemes. In particular CB gives dispersed curves, which might indicate that the approximations are not good on W_2.

Table 3.7 gives the wall stress on W_2 for $Re = 0, 250$ and 500. For the same range of the Reynolds number the widths for the upper vortex are given in Table 3.8.

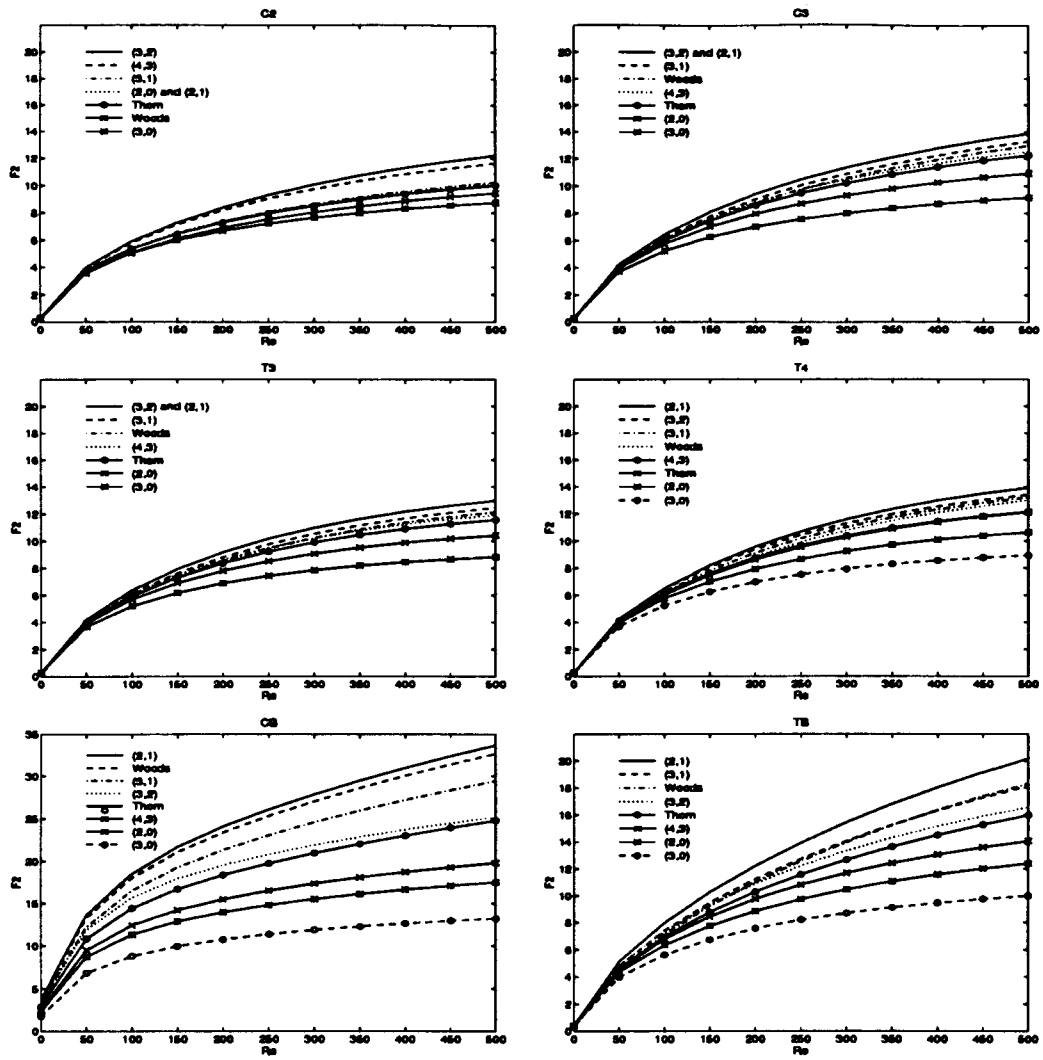

Figure 3.7: Stress on wall W_2 for different schemes and vorticity boundary approximations.

The values for the boundary stress F_3 on W_3 are plotted in Figure 3.8. The value of F_3 decreases from the first-order to the second-order formulae. A fairly good agreement among the boundary vorticity conditions for $Re \leq 50$ is found. Now Woods' boundary condition gives the smallest stress values overall. In reference [12], Gupta and Manohar described that Woods' boundary condition had the tendency to over-estimate the stress values on the moving boundary for the square cavity problem.

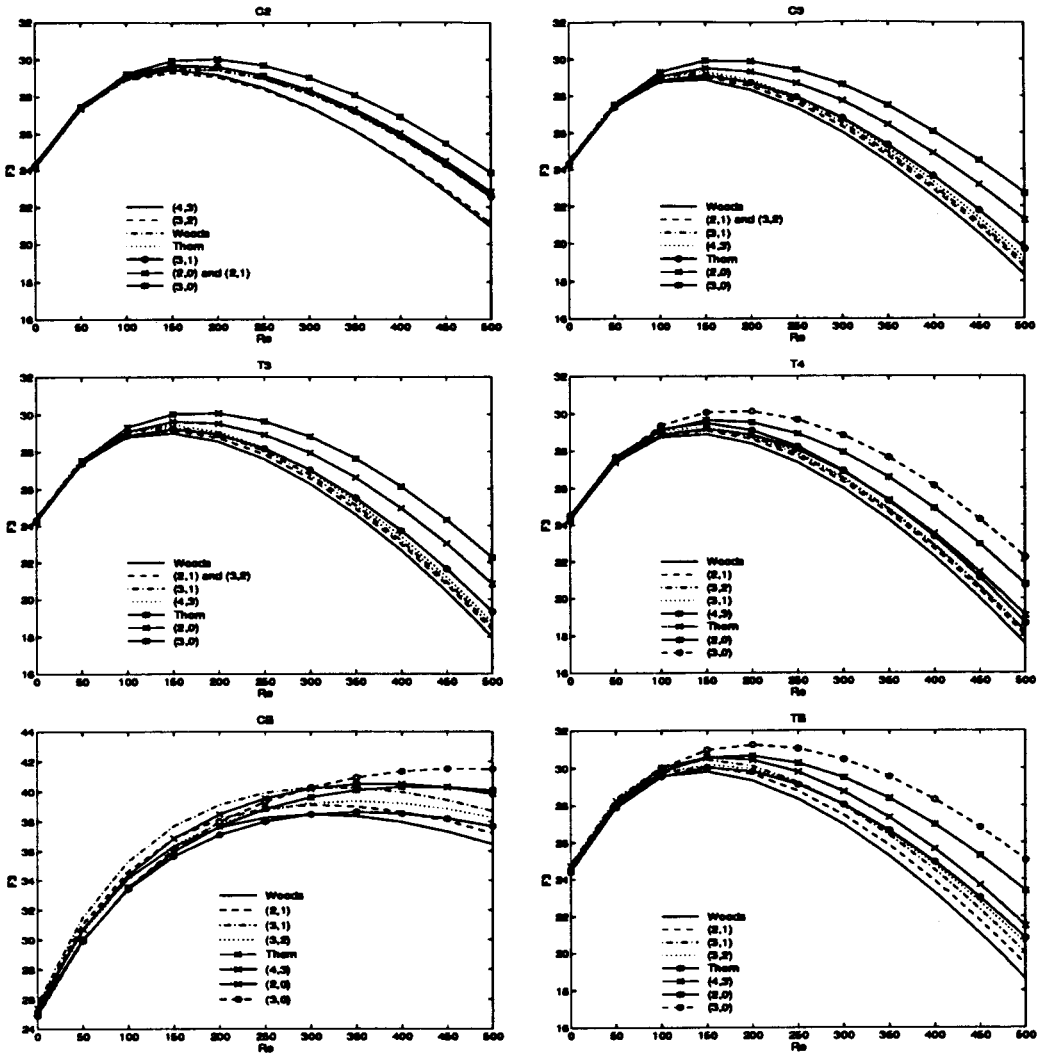

Figure 3.8: Stress on wall W_3 for different schemes and vorticity boundary approximations.

We presume that the same behavior is present in this case. Woods' formula might be under-estimating the value of the stress on W_3. Since the upstream results are more reliable, and the same pattern is not observed on W_1 and W_2, we cannot assure that Woods' condition is "better" in this case. Values of F_3 for $Re = 0, 250$ and 500 are given in Table 3.9. Since the downstream recirculation region was not found for $Re \leq 250$, the values of L_3 and L_4 for $Re = 250$ and 500 are given in Table 3.10 and Table 3.11. Note that the plots for CB differ totally from the rest. This indicates that

scheme CB is not trustworthy on this boundary. A quick inspection of Table 3.10 and Table 3.11 shows that the length values obtained for this scheme disagree with the values obtained by other schemes.

In the case of the flow in a channel with a sudden contraction, as reported by Gupta and Manohar [12] for the cavity flow, there are differences in the values of the wall stress for different boundary vorticity conditions for a fixed scheme. The values of F_1 and F_3 decrease as the accuracy of the boundary condition increases. The opposite behavior is found for F_2.

Figure 3.9 gives the vorticity distribution on W_3 for $Re = 250$ and $Re = 500$.

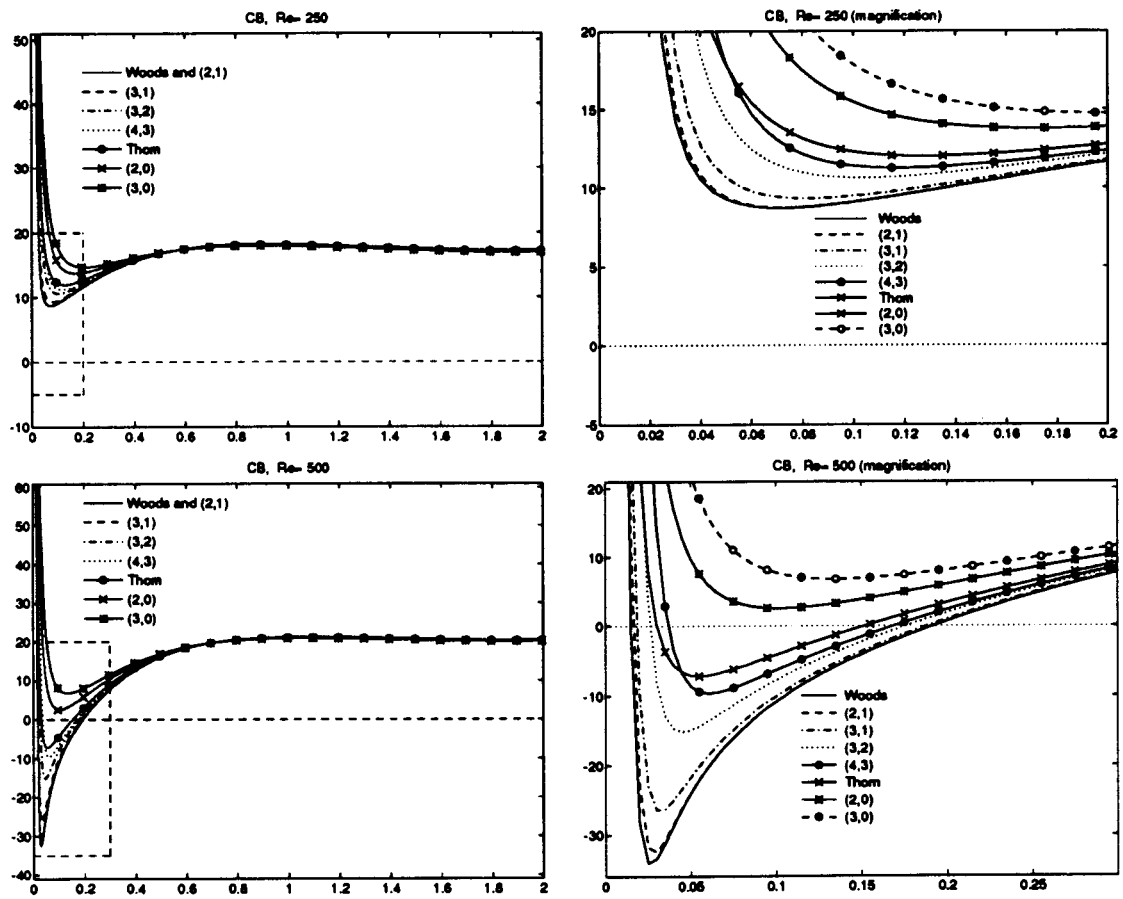

Figure 3.9: Vorticity distribution on wall W_3 for CB scheme ($Re = 250$ and 500).

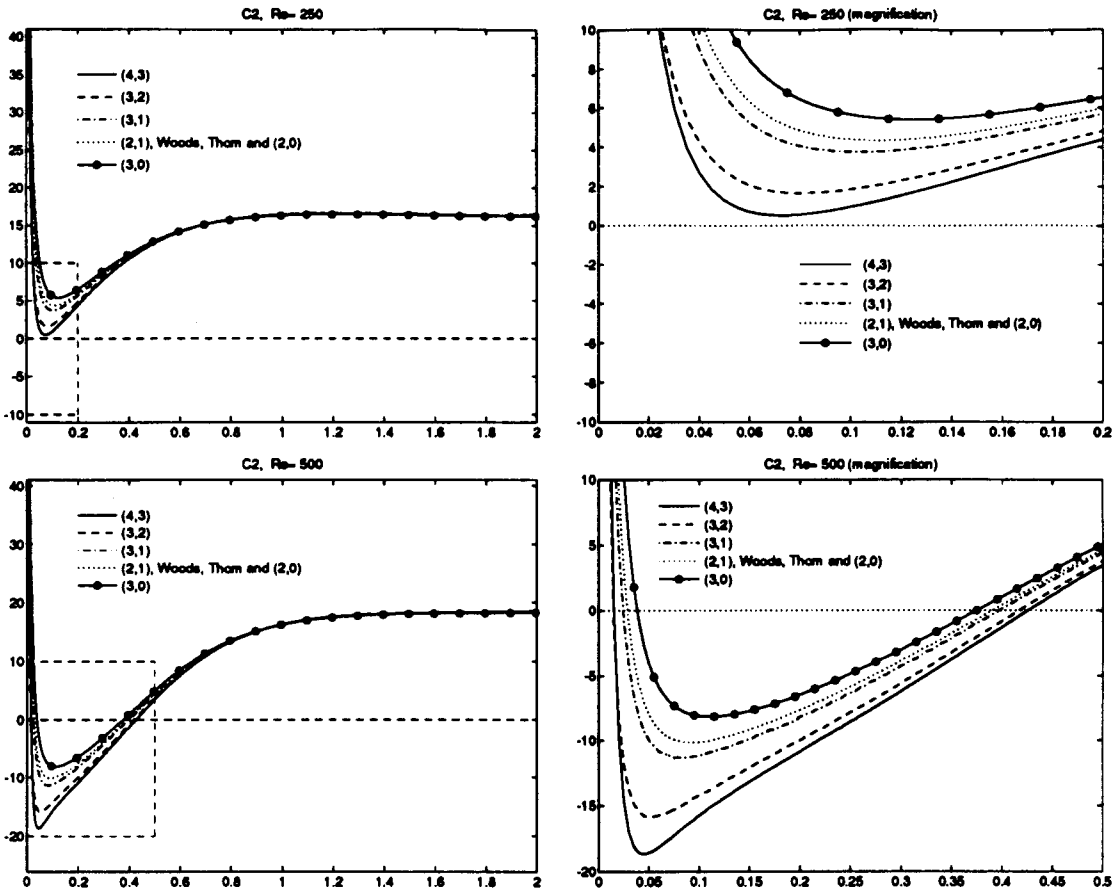

Figure 3.10: Vorticity distribution on wall W_3 for C2 scheme ($Re = 250$ and 500).

Examining the plots we conclude that scheme CB does not reproduce the expected behavior, which is in agreement with the results previously found for the stress on that boundary.

The (4,3) boundary formula suits the best scheme C2. However, this scheme is unable to capture the recirculation region for $Re = 250$ (see Figure 3.10).

Scheme C3 employs the same interior approximation as scheme C2. They only differ in the order of the extrapolation formula for the stream function on the computational boundary. The use of a third-order formula changes dramatically the solution (see Figure 3.11).

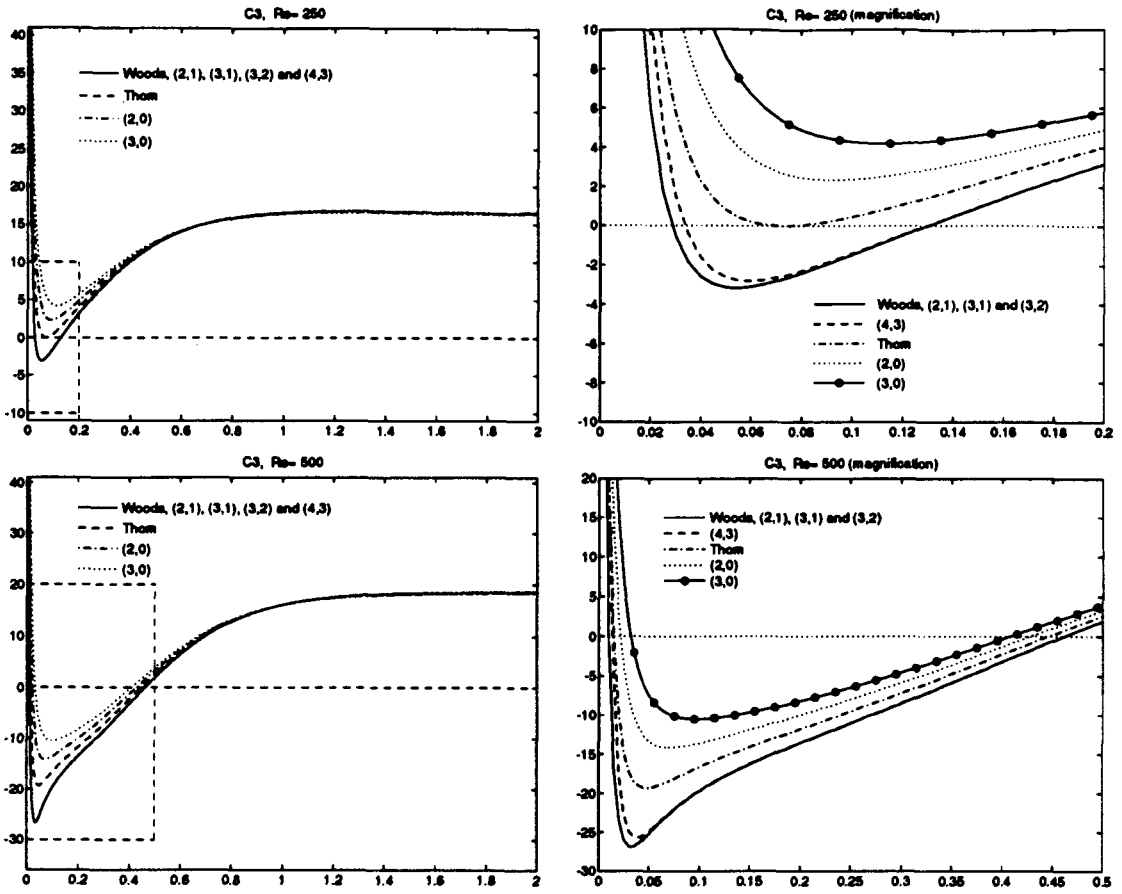

Figure 3.11: Vorticity distribution on wall W_3 for C3 scheme ($Re = 250$ and 500).

Now the recirculation region is visible for $Re = 250$. Also note that now for Thom's formula the boundary vorticity comes close to zero at $Re = 250$. This means that Thom's formula is not good enough to produce recirculation downstream, but clearly is the best of all first-order formulae. The analysis of the boundary stress suggests that the (3,2) boundary formula suits this scheme the best.

Schemes T3 and T4 produce very close results (see Figure 3.12 and Figure 3.13). It seems that the order of the extrapolation formula used for the stream function on the computational boundary does not have a significant effect on the compact scheme.

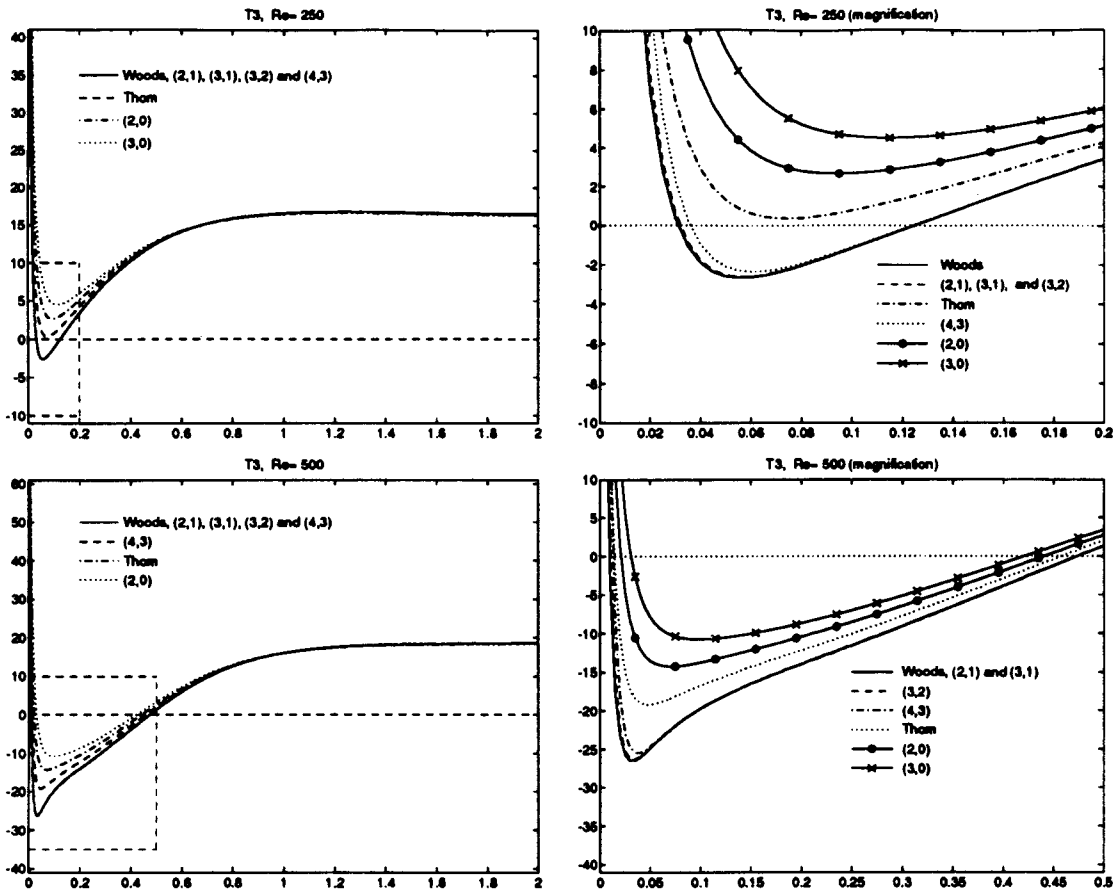

Figure 3.12: Vorticity distribution on wall W_3 for T3 scheme ($Re = 250$ and 500).

The only difference occurs for the (4,3) formula for both Reynolds numbers considered. Recall that the (4,3) formula is the less accurate of all second-order formulae. For both schemes the (3,2) vorticity boundary formula seems to work better. Furthermore, all the second-order formulae seem to work fine with this scheme. Based upon the results for the stress on the boundaries the (3,2) formula has been chosen as the most reliable.

There is a significant difference in the minimum value of the boundary vorticity for both values of Reynolds numbers $Re = 250$ and $Re = 500$. The more accurate the scheme, the smaller the minimum value become.

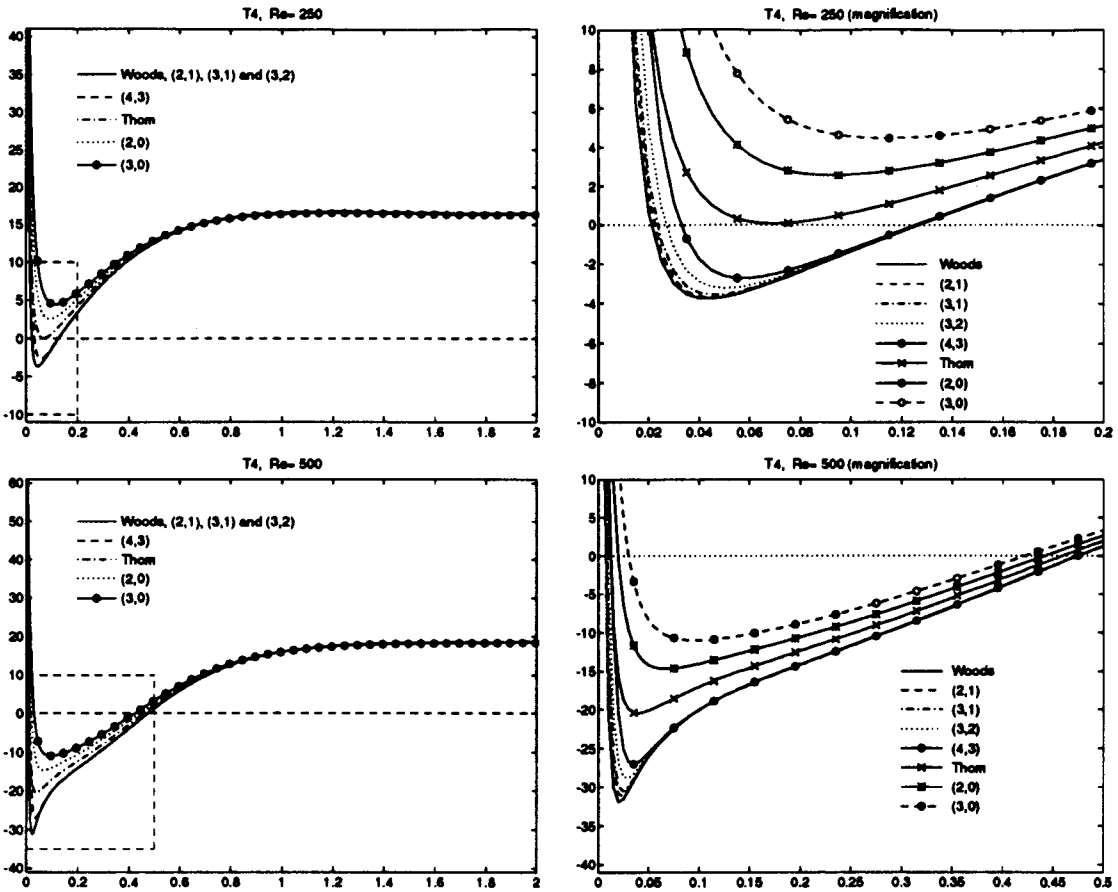

Figure 3.13: Vorticity distribution on wall W_3 for T4 scheme ($Re = 250$ and 500).

Note that none of the first-order formulae reproduced the wake after the contraction for $Re = 250$. Also Thom's formula seems to be the best of these.

The TB scheme produces a very small wake for Thom's formula at $Re = 250$ (see Figure 3.14). This scheme gives the smallest vorticity values of all at the boundary W_3, and the (2,1) formula seems to work well with this scheme.

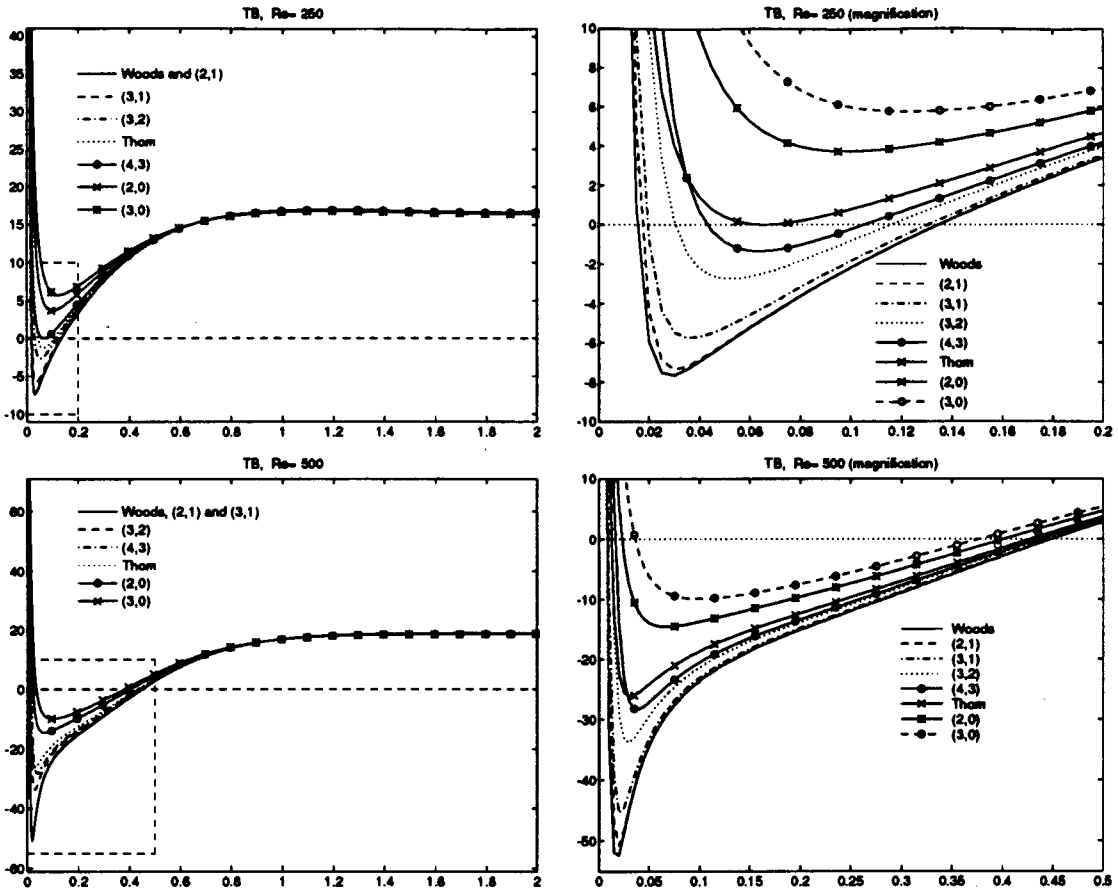

Figure 3.14: Vorticity distribution on wall W_3 for TB scheme ($Re = 250$ and 500).

So far we have determined which vorticity boundary approximation is best to use with each scheme. All the boundary formulae chosen are of second-order of accuracy.

An interesting feature occurs near the upper corner for every scheme. An oscillation of the vorticity values is observed for most of the second-order formulae. Figure 3.15 shows the vorticity values for scheme T4 for two second-order boundary formulae at $Re = 500$. Formula (4,3) behaves in the same way formula (3,2) does on this plot. The rest of the second-order formulae, and the first-order Thom's formula, give a similar behavior to the shown in Figure 3.15 for formula (2,1).

Figure 3.16 shows the boundary vorticity values for $Re = 0, 150, 250, 350$ and 500 on W_1 and on W_3 for schemes C3, T3 and TB. Formula (2,0) is used for the plots on

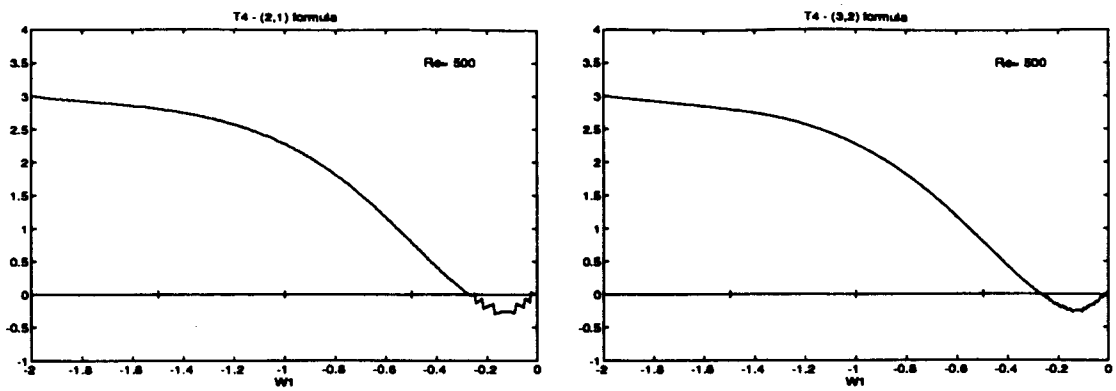

Figure 3.15: Oscillations of the vorticity distribution on wall W_1 for scheme T4 .

W_1 and the (3,2) formula for the plots on W_3. TB uses the (2,1) formula on W_3.

Figure 3.6 and Figure 3.8 might lead us to think that F_1 has a maximum for $0 < Re < 50$ and that F_3 has a maximum for $100 < Re < 200$. Further calculations were made in that range of Reynolds number using the T4 scheme. It was found that F_1 attains the maximum value of 4.487 at $Re = 15$ and that F_3 attains a maximum of 29.189 at $Re = 140$. The values of the Reynolds number at which the wall stress attains a maximum on W_3 might be related to the value of the Reynolds number at which the recirculation first appears.

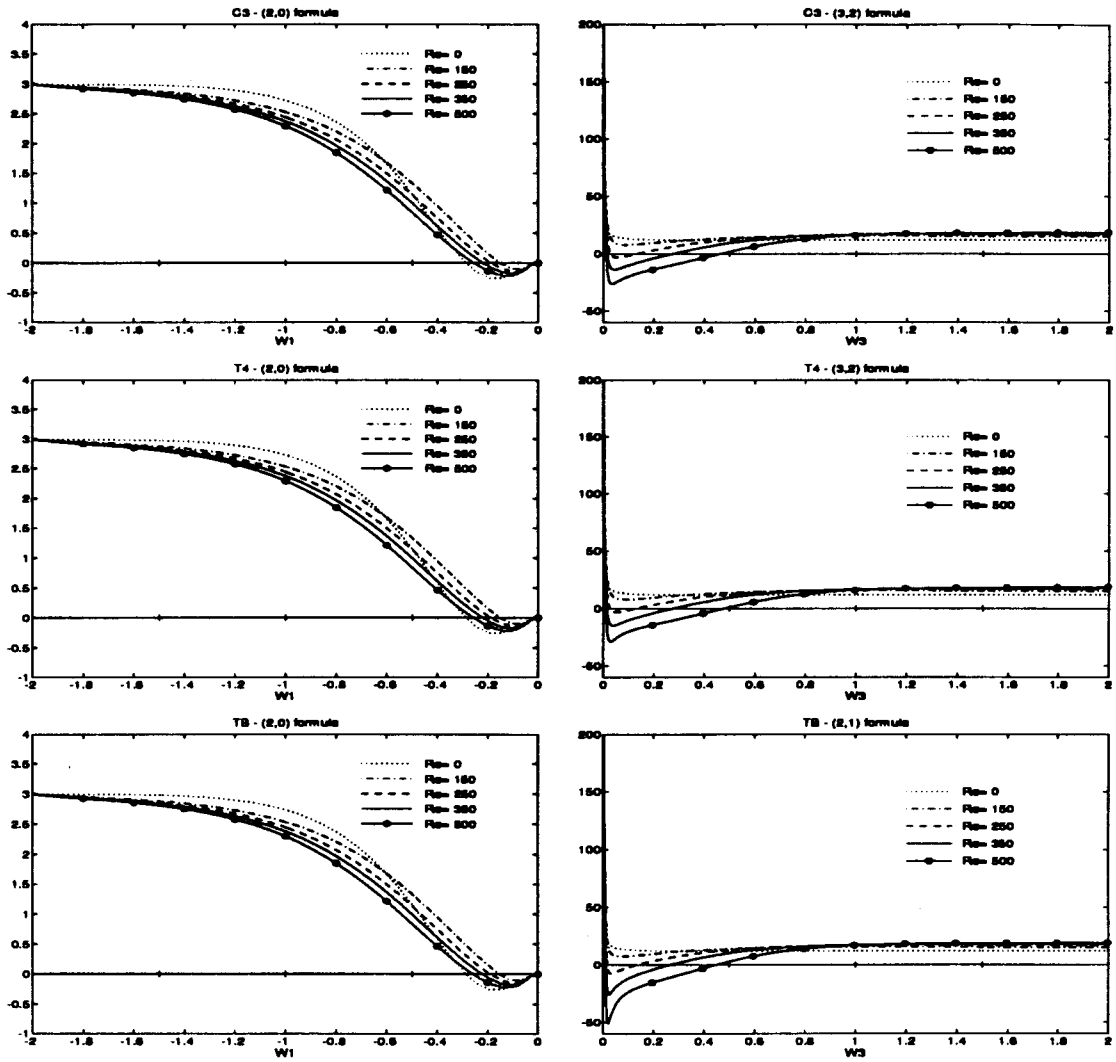

Figure 3.16: Vorticity distribution on walls W_1 and W_3 for schemes C3, T4 and TB.

3.5.2 Length of Recirculation Regions

Figure 3.17 shows the streamline contours for different values of Re. The calculations were made using the compact scheme and fourth-order extrapolation on the boundary. A magnification of the streamlines and vorticity contours near the re-entrant corner is also given (see Figure 3.18).

Let us first consider the solution upstream of the step. The vortex in the upper corner is present for all values of Re. Fine meshes are not necessary to obtain reliable results. In reference [10] Friedman obtained this vortex using $h = \frac{1}{40}$. He stated that the vortex reduces its size when $0 \leq Re \leq Re_{min}$ with $10 < Re_{min} < 50$, and increases monotonically for $Re > Re_{min}$.

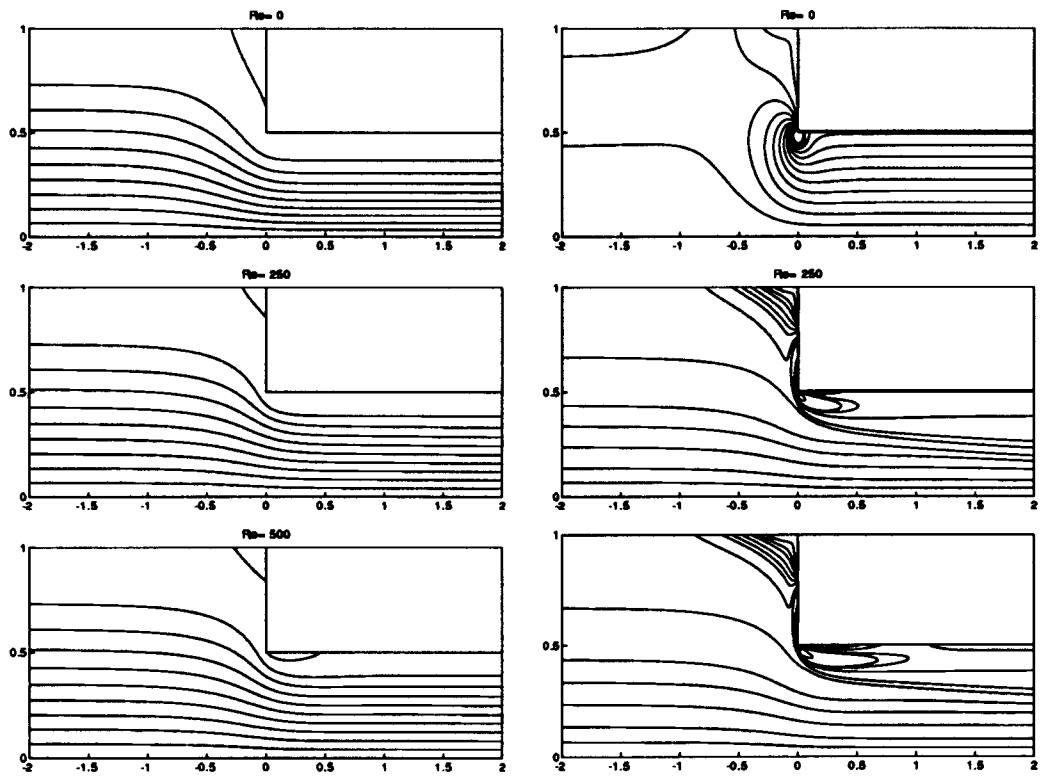

Figure 3.17: Streamlines and vorticity contours for scheme T4-(3,2).

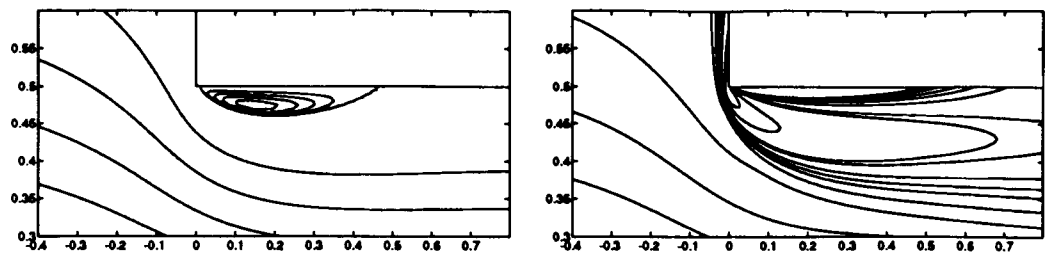

Figure 3.18: Magnification of streamlines and vorticity contours for $Re = 500$ near the re-entrant corner for scheme T4-(3,2).

Dennis and Smith [8] used mesh size $h = \frac{1}{60}$ and found that L_1 attains a minimum at about $Re = 50$, and it increases monotonically for $50 < Re < 2000$. They also produced the vortex length and width for different values of Re. In reference [22] Karageorghis and Phillips set the minimum value of L_1 at $Re = 45$. Our calculations using the scheme T4 and (3,2) formula show that $Re_{min} = 45$ and the wake length L_1 is 0.1286.

In Table 3.1 and Table 3.2 the values for L_1 and L_2 as well as those previously obtained by other authors are shown. In general L_1 and L_2 show good agreement.

Re	0	1	50	100	250	500
Dennis & Smith [8]	0.284	0.255	0.129	0.144	—	0.275
Hunt (upwind) [20]	—	—	—	—	0.209	0.260
Hunt (central) [20]	—	—	—	—	0.227	0.308
Karageorghis & Phillips [8]	0.290	—	0.123	0.144	0.205	0.265
Hawken *et al.* [15]	—	0.261	0.128	—	0.205	0.285
Huang & Seymour [19]	—	—	—	0.145	0.205	0.275
Burggraf [19]	—	—	—	0.145	0.202	0.271
Dennis & Smith [19]	—	—	—	—	—	0.273
C3-(3,2)	0.296	—	0.129	0.144	0.205	0.277
T4-(3,2)	0.296	0.265	0.129	0.144	0.205	0.276
TB-(2,1)	0.299	—	0.136	0.151	0.209	0.285

Table 3.1: Separation point at upper corner (L_1).

Re	0	1	50	100	250	500
Dennis & Smith [8]	—	—	—	—	—	—
Hunt (upwind) [20]	—	—	—	—	0.138	0.149
Hunt (central) [20]	—	—	—	—	0.145	0.164
Karageorghis & Phillips [8]	—	—	—	—	—	—
Hawken *et al.* [15]	—	0.327	0.118	—	0.138	0.154
Huang & Seymour [19]	—	—	—	0.126	0.143	0.161
Burggraf [19]	—	—	—	0.126	0.142	0.161
Dennis & Smith [19]	—	—	—	—	—	0.162
C3-(3,2)	0.380	—	0.123	0.125	0.142	0.162
T4-(3,2)	0.380	0.332	0.122	0.125	0.141	0.162
TB-(2,1)	0.387	—	0.115	0.120	0.146	0.164

Table 3.2: Reattachment point at the upper corner (L_2).

Karageorghis and Phillips [22], observed a second vortex near the upper corner for Reynolds number as low as $Re = 10$. This second vortex was not observed in our calculations.

The most interesting and controversial feature for the flow channel appears at the re-entrant corner. A downstream recirculation region is formed after the tip of the corner. Dennis and Smith in their early work [8], obtained a downstream eddy formation for $Re = 1000$ and $Re = 2000$ with $h = \frac{1}{80}$. They predicted a recirculating flow for $Re = 500$ with separation at a point on the interval $0 < x < 0.3$ and reattachement point to the right of $x = 1.2$. They were certain that no downstream separation occurs for $0 \leq Re \leq 100$ and therefore such separation must occur for $100 < Re < 500$. Hunt [20] found a downstream vortex for Re= 250, with separation to the right of the corner. Karageorghis and Phillips [22] placed the apparition of the recirculating flow at about $Re = 175$, with separation at the corner. Their reattachement values 0.500 and 0.995 are larger than the values obtained by other authors.

In reference [15] Hawken employed a finite element method for primitive variables formulation. He predicted a vortex, with separation to the right of the corner, starting at $Re = 250$. His values are slightly larger than predicted by Hunt.

Re	250	350	450	500
Dennis & Smith [8]	0.000	0.000	0.000	0.000
Hunt (upwind) [20]	0.018	—	—	0.006
Hunt (central) [20]	0.023	—	—	0.008
Karageorghis & Phillips [8]	0.000	0.000	0.000	0.000
Hawken *et al.* [15]	0.080	0.053	0.042	0.037
Huang & Seymour [19]	—	—	—	—
Burggraf [19]	—	—	—	—
Dennis & Smith [19]	—	—	—	—
C3-(3,2)	0.029	0.016	0.013	0.011
T4-(3,2)	0.027	0.015	0.011	0.010
TB-(2,1)	0.018	0.012	0.010	0.009

Table 3.3: Separation point after the re-entrant corner (L_3).

Huang and Seymour [19] also predicted separation after the corner for $Re \geq 250$. Their results are in good agreement with Hunt's and Hawken's. Tables 3.3 and 3.4 show the values of L_3 and L_4 predicted by our calculations, together with the results previously reported in the literature. Our calculations show that there is a downstream recirculation region for $Re = 250$, with separation to the right of the corner. In general the values produced by scheme TB are slightly higher that those produced by the other schemes.

Re	250	350	450	500
Dennis & Smith [8]	0.000	0.000	0.000	0.000
Hunt (upwind) [20]	0.124	—	—	0.412
Hunt (central) [20]	0.119	—	—	0.414
Karageorghis & Phillips [8]	0.500	0.700	0.924	0.995
Hawken *et al.* [15]	0.155	0.301	0.423	0.477
Huang & Seymour [19]	0.126	—	—	0.444
Burggraf [19]	0.079	—	—	0.415
Dennis & Smith [19]	—	—	—	0.413
C3-(3,2)	0.130	0.274	0.400	0.461
T4-(3,2)	0.126	0.273	0.407	0.475
TB-(2,1)	0.135	0.267	0.388	0.449

Table 3.4: Reattachment point after the re-entrant corner (L_4).

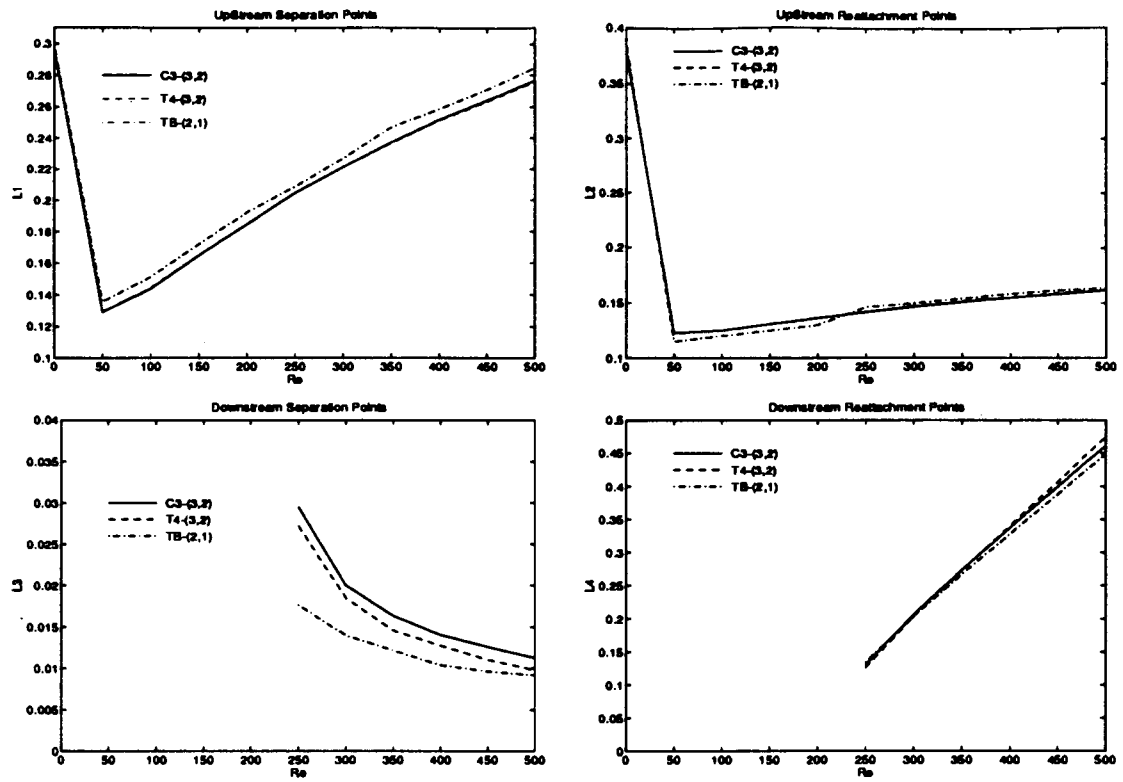

Figure 3.19: Characteristic lengths.

The value at which the downstream vortex first appears is not certain yet. The recent works show a recirculating flow starting at $Re = 250$, except for Karageorghis and Phillips' which first appears at about $Re = 175$. Obviously this problem is still open.

Figure 3.19 shows the plots of the characteristic lengths versus the Reynolds number. The plots are given for the schemes C3, T4 and TB. These results are in agreement with experimental ones produced by Durst and Loy [9] for a circular cylinder.

Tables

	BC1	BC2	BC3	BC4	BC5	BC6	BC7	BC8
$Re = 0$								
C2	4.053	4.059	4.053	4.056	4.054	4.059	4.056	4.062
C3	4.060	4.069	4.056	4.059	4.064	4.069	4.060	4.066
T3	4.060	4.069	4.056	4.059	4.064	4.069	4.061	4.066
T4	4.060	4.069	4.057	4.060	4.064	4.069	4.061	4.067
CB	4.158	4.166	4.154	4.155	4.162	4.166	4.160	4.164
TB	4.070	4.079	4.066	4.068	4.074	4.079	4.072	4.075
$Re = 250$								
C2	3.894	3.898	3.894	3.905	3.893	3.895	3.881	3.881
C3	3.874	3.870	3.885	3.900	3.864	3.870	3.865	3.871
T3	3.875	3.870	3.885	3.900	3.864	3.870	3.865	3.871
T4	3.875	3.870	3.886	3.901	3.865	3.870	3.865	3.871
CB	3.904	3.893	3.919	3.936	3.888	3.895	3.897	3.904
TB	3.872	3.862	3.887	3.904	3.857	3.863	3.864	3.872
$Re = 500$								
C2	3.638	3.643	3.638	3.654	3.639	3.638	3.616	3.612
C3	3.605	3.593	3.621	3.643	3.588	3.593	3.588	3.593
T3	3.602	3.590	3.619	3.641	3.585	3.590	3.585	3.591
T4	3.602	3.590	3.620	3.641	3.585	3.590	3.586	3.591
CB	3.636	3.615	3.661	3.686	3.611	3.618	3.622	3.632
TB	3.598	3.577	3.623	3.647	3.572	3.580	3.584	3.593

Table 3.5: Stress values on boundary W_1.

	BC1	BC2	BC3	BC4	BC5	BC6	BC7	BC8
$Re = 0$								
C2	0.285	0.279	0.289	0.287	0.279	0.279	0.292	0.293
C3	0.290	0.296	0.290	0.287	0.296	0.296	0.296	0.297
T3	0.290	0.296	0.290	0.287	0.296	0.296	0.296	0.296
T4	0.290	0.296	0.290	0.287	0.296	0.296	0.296	0.297
CB	0.265	0.269	0.260	0.257	0.269	0.268	0.267	0.266
TB	0.295	0.299	0.290	0.287	0.299	0.299	0.296	0.295
$Re = 250$								
C2	0.185	0.174	0.185	0.183	0.185	0.188	0.194	0.198
C3	0.195	0.205	0.190	0.185	0.206	0.205	0.205	0.204
T3	0.195	0.205	0.190	0.185	0.206	0.205	0.205	0.204
T4	0.195	0.205	0.190	0.185	0.206	0.205	0.205	0.204
CB	0.195	0.206	0.185	0.180	0.206	0.205	0.201	0.199
TB	0.200	0.210	0.195	0.188	0.209	0.209	0.209	0.206
$Re = 500$								
C2	0.255	0.256	0.250	0.249	0.256	0.257	0.265	0.268
C3	0.270	0.277	0.260	0.253	0.277	0.277	0.277	0.276
cd T3	0.270	0.277	0.260	0.254	0.277	0.276	0.276	0.277
T4	0.270	0.277	0.260	0.254	0.277	0.277	0.276	0.276
CB	0.265	0.275	0.254	0.245	0.274	0.274	0.272	0.269
TB	0.275	0.285	0.260	0.254	0.285	0.284	0.281	0.278

Table 3.6: Separation values at the upper corner (L_1) for Re=0, 250 and 500.

	BC1	BC2	BC3	BC4	BC5	BC6	BC7	BC8
$Re = 0$								
C2	0.294	0.238	0.321	0.310	0.320	0.286	0.293	0.264
C3	0.271	0.189	0.320	0.313	0.284	0.252	0.283	0.261
T3	0.271	0.188	0.321	0.314	0.283	0.251	0.284	0.262
T4	0.268	0.177	0.325	0.318	0.277	0.246	0.286	0.265
CB	2.906	3.625	2.322	1.750	3.744	3.307	3.262	2.503
TB	0.380	0.269	0.430	0.402	0.440	0.374	0.421	0.374
$Re = 250$								
C2	7.992	7.558	8.092	7.235	8.095	8.095	9.325	9.056
C3	9.461	9.746	8.700	7.562	10.468	10.034	10.470	9.725
T3	9.220	9.470	8.524	7.451	10.173	9.763	10.175	9.513
T4	9.531	9.903	8.663	7.529	10.677	10.161	10.428	9.662
CB	19.759	25.340	14.803	11.358	26.111	23.075	20.826	16.504
TB	11.561	12.587	9.722	8.189	13.932	12.746	12.214	10.806
$Re = 500$								
C2	10.002	9.456	10.113	8.754	10.114	10.247	12.250	11.662
C3	12.268	12.958	10.929	9.154	13.871	13.287	13.873	12.543
T3	11.556	12.145	10.400	8.827	12.975	12.458	12.976	11.915
T4	12.139	13.005	10.628	8.944	13.933	13.220	13.413	12.157
CB	24.791	32.659	17.510	13.196	33.674	29.464	25.208	19.812
TB	15.987	18.333	12.409	9.987	20.162	18.157	16.566	14.077

Table 3.7: Stress values on boundary W_2.

	BC1	BC2	BC3	BC4	BC5	BC6	BC7	BC8
$Re = 0$								
C2	0.355	0.355	0.358	0.353	0.354	0.361	0.368	0.371
C3	0.370	0.380	0.364	0.356	0.380	0.380	0.380	0.380
T3	0.370	0.380	0.364	0.356	0.380	0.380	0.380	0.379
T4	0.370	0.381	0.363	0.356	0.380	0.380	0.380	0.379
CB	0.285	0.293	0.285	0.281	0.285	0.295	0.292	0.293
TB	0.370	0.387	0.362	0.353	0.387	0.385	0.380	0.377
$Re = 250$								
C2	0.130	0.130	0.134	0.132	0.129	0.130	0.137	0.138
C3	0.135	0.142	0.135	0.133	0.135	0.141	0.142	0.141
T3	0.135	0.142	0.135	0.133	0.135	0.141	0.142	0.141
T4	0.135	0.142	0.135	0.133	0.135	0.141	0.141	0.141
CB	0.125	0.125	0.125	0.124	0.125	0.127	0.127	0.129
TB	0.140	0.146	0.138	0.133	0.146	0.145	0.143	0.142
$Re = 500$								
C2	0.155	0.155	0.155	0.154	0.155	0.156	0.158	0.159
C3	0.160	0.162	0.157	0.155	0.162	0.162	0.162	0.161
T3	0.160	0.162	0.158	0.155	0.162	0.162	0.162	0.162
T4	0.160	0.163	0.158	0.155	0.162	0.162	0.162	0.162
CB	0.145	0.144	0.145	0.145	0.145	0.145	0.145	0.148
TB	0.160	0.165	0.158	0.155	0.164	0.163	0.163	0.162

Table 3.8: Reattachment values at the upper corner (L_2) for Re=0, 250 and 500.

	BC1	BC2	BC3	BC4	BC5	BC6	BC7	BC8
$Re = 0$								
C2	24.163	24.204	24.182	24.189	24.179	24.275	24.297	24.412
C3	24.346	24.478	24.280	24.259	24.454	24.528	24.453	24.531
T3	24.330	24.470	24.247	24.231	24.412	24.486	24.411	24.495
T4	24.330	24.466	24.251	24.235	24.408	24.486	24.415	24.501
CB	25.123	25.512	24.974	24.887	25.597	25.758	25.355	25.390
TB	24.574	24.810	24.446	24.398	24.789	24.876	24.689	24.736
$Re = 250$								
C2	28.981	28.957	29.145	29.692	29.145	29.134	28.400	28.483
C3	27.941	27.351	28.702	29.425	27.619	27.811	27.618	27.983
T3	28.046	27.543	28.613	29.364	27.478	27.674	27.478	27.884
T4	27.913	27.269	28.592	29.375	27.234	27.472	27.400	27.866
CB	37.996	38.263	38.844	39.322	38.867	39.934	38.766	39.558
TB	29.124	28.343	30.270	31.039	28.771	29.247	29.199	29.790
$Re = 500$								
C2	22.612	22.537	22.822	23.864	22.822	22.571	21.113	20.927
C3	19.697	18.304	21.239	22.686	18.728	18.903	18.729	19.166
T3	19.168	17.886	20.453	21.926	17.883	18.052	17.881	18.342
T4	18.881	17.391	20.325	21.847	17.438	17.654	17.663	18.206
CB	37.654	36.455	40.079	41.500	37.194	38.680	38.237	39.843
TB	20.815	18.612	23.353	25.040	19.364	19.992	20.495	21.474

Table 3.9: Stress values on boundary W_3.

	BC1	BC2	BC3	BC4	BC5	BC6	BC7	BC8
$Re = 250$								
C2	0.000	0.000	0.000	0.000	0.000	0.000	0.000	0.000
C3	0.070	0.029	0.000	0.000	0.030	0.029	0.029	0.034
T3	0.000	0.031	0.000	0.000	0.032	0.032	0.032	0.036
T4	0.000	0.021	0.000	0.000	0.023	0.024	0.027	0.033
CB	0.000	0.000	0.000	0.000	0.000	0.000	0.000	0.000
TB	0.065	0.016	0.000	0.000	0.018	0.020	0.031	0.043
$Re = 500$								
C2	0.029	0.028	0.029	0.038	0.029	0.024	0.015	0.015
C3	0.015	0.010	0.022	0.032	0.011	0.011	0.011	0.014
T3	0.015	0.010	0.021	0.031	0.011	0.011	0.011	0.013
T4	0.012	0.007	0.020	0.030	0.009	0.009	0.010	0.013
CB	0.030	0.015	0.000	0.000	0.017	0.019	0.027	0.037
TB	0.013	0.008	0.023	0.036	0.009	0.010	0.013	0.017

Table 3.10: Separation values after the re-entrant corner (L_3) for $Re = 250$ and 500.

	BC1	BC2	BC3	BC4	BC5	BC6	BC7	BC8
$Re = 250$								
C2	0.000	0.000	0.000	0.000	0.000	0.000	0.000	0.000
C3	0.075	0.130	0.000	0.000	0.130	0.130	0.130	0.130
T3	0.000	0.125	0.000	0.000	0.125	0.125	0.125	0.124
T4	0.000	0.127	0.000	0.000	0.127	0.126	0.126	0.125
CB	0.000	0.000	0.000	0.000	0.000	0.000	0.000	0.000
TB	0.065	0.135	0.000	0.000	0.135	0.131	0.116	0.106
$Re = 500$								
C2	0.390	0.390	0.390	0.375	0.390	0.398	0.417	0.426
C3	0.445	0.461	0.428	0.408	0.461	0.461	0.461	0.462
T3	0.458	0.474	0.440	0.421	0.474	0.474	0.474	0.473
T4	0.459	0.475	0.442	0.422	0.475	0.475	0.475	0.475
CB	0.152	0.192	0.000	0.000	0.192	0.188	0.176	0.169
TB	0.427	0.449	0.401	0.377	0.449	0.447	0.439	0.436

Table 3.11: Reattachment values after the re-entrant corner (L_4) for $Re = 250$ and 500.

Chapter 4

Conclusions

In this thesis we have studied the flow through a constricted channel for moderate-high Reynolds number. The Interior Constraint (IC) Method and the Vorticity Interior Constraint (VIC) Method were employed to solve the steady Navier-Stokes equations. Both methods were applied using a second-order central difference scheme and a fourth-order compact scheme. The results show that, for the second-order method, an increase of the order for the stream function extrapolation formula, from second to third-order, produces a qualitative change in the solution. The solution using the compact scheme is not visibly affected by an increase of order for the extrapolation formula from third to fourth-order. The compact scheme allows the use of over-relaxation and the number of SOR iterations is reduced considerably. It also allows us to compute solutions for higher values of the Reynolds number. Iteration-wise the VIC method is similar to the IC method for both schemes.

Several vorticity boundary approximations are tested for each method. The analysis of the boundary stress allows us to choose the most adequate boundary formula. Several flow parameters, e.g. separation and reattachement points, are also calculated, and comparisons with published results are given. Our results show that the combination of the VIC method and the second order central differences scheme is not suitable to solve this problem. The compact scheme seems to work well for both IC and VIC methods. The results obtained, for each case, agree qualitatively with

experiments carried out for a circular cylinder.

There are still several open questions for this problem. The most important one is to determine the value of the Reynolds number at which the downstream recirculation region first appears.

Some possible future improvements of this work are the following

- To analize of a higher order approximation for the stream function at the grid points adjacent to the boundary for the VIC method.
- To use the most reliable scheme and boundary vorticity to investigate the solutions for higher values of Reynolds numbers.

Bibliography

[1] G. K. Batchelor. *An Introduction to Fluid Dynamics.* Cambridge Univ. Press, 1967.

[2] J. S. Bramley and S. C. R. Dennis. The numerical solution of two-dimensional flow in a branching channel. *Computers and Fluids*, 12(4):339–355, 1984.

[3] J. S. Bramley and D. Sloan. A comparison of an upwind difference scheme with a central difference scheme for moderate reynolds number. Technical Report 3, Department of Mathematics, The University of Strathclyde, Glasgow, Scotland, 1988.

[4] L. Collatz. *The Numerical Treatment of Differential Equations.* Springer-Verlag, Berlin/New York, 3rd edition, 1966.

[5] I. G. Currie. *Fundamental Mechanics of Fluids.* McGraw-Hill Inc., 1974.

[6] B. P. Demidovich and I. A. Maron. *Computational Mathematics.* MIR Publishers, Moscow, Russia, 1973.

[7] S. C. R. Dennis and J. D. Hudson. A difference method for solving the Navier Stokes equations. In *Proc. 1st Conf. on Numerical Methods in Laminar and Turbulent Flow.* Pentech Press, London, 1978.

[8] S. C. R. Dennis and F. T. Smith. Steady flow through a channel with a symmetrical constriction in the form of a step. *Proceedings Royal Society London A*, 372:393–414, 1980.

[9] F. Durst and T. Loy. Investigations of laminar flow in a pipe with sudden contraction of cross sectional area. *Computers and Fluids*, 13(1):15–36, 1985.

[10] M. Friedman. Laminar flow in a channel with step. *Journal of Engineering Mathematics*, 6(3):285–290, July 1972.

[11] D. Greenspan. Numerical studies of steady, viscous, incompressible flow in a channel with step. *Journal of Engineering Mathematics*, 3(1):21–28, January 1969.

[12] M. M. Gupta and R. P. Manohar. Boundary approximations and accuracy in viscous flows computations. *Journal of Computational Physics*, 31:265–288, 1979.

[13] M. M. Gupta and R. P. Manohar. On the use of central difference scheme for Navier Stokes equations. *International Journal for Numerical Methods in Engineering*, 15:557–573, 1980.

[14] M. M. Gupta, R. P. Manohar, and B. Noble. Nature of viscous flows near sharp corners. *Computers and Fluids*, 9(4):379–388, 1981.

[15] D. M. Hawken, P. Townsend, and M. F. Webster. Numerical simulation of viscous flows in channels with a step. *Computers and Fluids*, 20(1):59–75, 1991.

[16] S. Hou, J. Sterling, S. Shen, and G. D. Doolen. A lattice Boltzmann subgrid model for high Reynolds number flows. Theoretical Division and Center for Nonliner Studies, Los Alamos National Laboratory, Los Alamos, 1994.

[17] S. Hou, Q. Zou, S. Chen, G. D. Doolen, and A. Cogley. Navier Stokes fluid flows using a lattice Boltzmann method. (submitted to Journal of Computational Physics), 1994.

[18] H. Huang. *Incompressible Viscous Flow in Tubes with Occlusions.* PhD thesis, The University of British Columbia, Vancouver, B.C., Canada, 1991.

[19] H. Huang and B. R. Seymour. A finite difference method for flow in a constricted channel. (to appear in Computers and Fluids), 1993.

[20] R. Hunt. The numerical solution of the laminar flow in a constricted channel at moderately high Reynolds number using Newton iteration. *International Journal for Numerical Methods in Fluids*, 11:247–259, 1990.

[21] L. V. Kantorovich and V. I. Krylov. *Approximate Methods for Higher Analysis.* P. Noordhoff Ltd., Groninger, Groninger, The Netherlands, 1958.

[22] A. Karageorghis and T. N. Phillips. Conforming Chebyshev spectral collocation methods for the solution of laminar flow in a constricted channel. *IMA Journal of Numerical Analysis*, 11:33–54, 1991.

[23] M. Li, T. Tang, and B. Fornberg. A compact fourth order finite difference scheme for the steady, incompressible Navier Stokes equations. Technical Report #93-13, Deptartment of Mathematics and Statistics, Simon Fraser University, Burnaby, B.C., Canada, 1993.

[24] H. Ma and D. W. Ruth. A new scheme for vorticity computations near a sharp corner. *Computers and Fluids*, 23(1):23–38, 1994.

[25] H. K. Moffat. Viscous and resistive eddies near a sharp corner. *Journal of Fluid Mechanics*, 18:1–18, 1964.

[26] J. Paris and S. Whitaker. Confined wakes: A numerical solution of the Navier Stokes equations. *American Institute of Chemical Engineers Journal*, 11(6):1033–1041, 1965.

[27] P. J. Roache. *Computational Fluid Dynamics.* Hermosa Publishers, Albuquerque, New Mexico, 1972.

[28] A. Thom. The flow past a circular cylinder at low speeds. *Proc. Royal Soc. London, A*, 141:651, 1933.

[29] A. Wittkopf. High Order Wide and Compact Schemes for the Steady Incompressible Navier Stokes Equations. Master's thesis, Department of Mathematics and Statistics, Simon Fraser University, Burnaby, B.C., Canada, March 1994.

[30] S. Wolfram. Cellular automaton fluids 1: Basic Teory. *Journal of Statistical Physics*, 45(3/4):471–526, 1986.

[31] L. C. Woods. A note on the numerical solution of fourth order differential equations. *The Aeronautical Quarterly*, 5:176–184, 1954.